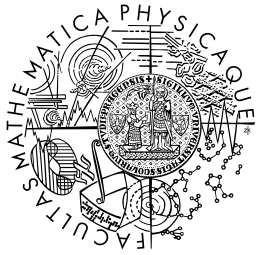

FACULTY
OF MATHEMATICS
AND PHYSICS
Charles University

MASTER THESIS

Jan Kára

Flare stars

Astronomical Institute of Charles University

Supervisor of the master thesis:	doc. RNDr. Marek Wolf, CSc.
Study programme:	Physics
Study branch:	Astronomy and Astrophysics

Prague 2018

I declare that I carried out this master thesis independently, and only with the cited sources, literature and other professional sources.

I understand that my work relates to the rights and obligations under the Act No. 121/2000 Sb., the Copyright Act, as amended, in particular the fact that the Charles University has the right to conclude a license agreement on the use of this work as a school work pursuant to Section 60 subsection 1 of the Copyright Act.

In ..... date ..... signature of the author

Title: Flare stars

Author: Jan Kára

Institute: Astronomical Institute of Charles University

Supervisor: doc. RNDr. Marek Wolf, CSc., Astronomical Institute of Charles University

Abstract: The works deals with the study of the flare stars, which is a group of stars for which sudden brightening can be observed. The work focuses on a star GJ 3236, which is a low-mass eclipsing binary and on which numerous flares have been observed. For the analysis of this system spectroscopic and photometric data were used, which were obtained at various observatories. Parameters of the binary system have been determined by analysing spectroscopic and photometric data with the program PHOEBE. A total of 241 flares have been detected in the photometric data and for 190 flares, which light curves were not affected by eclipses, released energies were estimated. The set of flares was used for the study of stellar activity of the binary. The energy distribution of observed flares is similar to the flares observed on other flare stars and also on the Sun. This suggests, that the flare mechanism is the same for these stars.

Keywords: flares, flare stars, low-mass eclipsing binaries, red dwarfs

I would like to thank my supervisor doc. RNDr. Marek Wolf, CSc. for patient guidance during my work on this diploma thesis.

I would like to thank also to my consultant Mgr. Tereza Klocová, Ph.D. for introducing me to the analysis of the spectroscopic data using the IRAF software.

The work would not be possible to make without the observation data obtained at various observatories and I would like to thank all observers who participated in the observations, namely Dr. Sergey Zharikov (San Pedro Mártir Observatory), Mgr. Hana Kučáková, Mgr. Kateřina Hoňková, RNDr. Jan Vraštil, Kamil Hornoch, doc. RNDr. Marek Wolf, CSc. (Ondřejov Observatory), Ladislav Šmelcer (Valašské Meziříčí Observatory), František Bílek (Trhové Sviny Observatory), Mgr. Marek Skarka Ph.D. (Piszkéstetö Observatory) and Pavol Dubovský (Kolonické sedlo Observatory). I would like to thank doc. Mgr. Štefan Parimucha, PhD. for providing me the observations obtained at the Kolonické sedlo Observatory.

Last but not least I would like to thank doc. Mgr. Michal Švanda, Ph.D. for useful advices on the topic of flares.

Contents

Introduction

Flares are enormous releases of energy which are connected to the magnetic activity of a star. The flares are observed as sudden brightening of a star, which can happen under 1 minute, which is than followed by much slower decrease, which can take up to several hours. Flares can be observed on stars of various spectral types and they are observed also on the Sun.

Thanks to the high spatial resolution of observation of the Sun, one can study the mechanism propelling flares in detail. Releases of energy associated with flares observed on other stars can be larger in several orders of magnitude than are the ones associated with the solar flares, the mechanism of the flares is however assumed to be the same. Flare stars therefore offer opportunity to study flares associated with a wide range of energies and also opportunity to study the stellar activity of a large sample of stars.

The Sun is known to have a 22-year cycle of decreasing and increasing solar activity with activity maximum happening each 11 years. The activity cycle can be monitored by the amount, size, position and polarity of the sunspots or by the amount and size of the flares. Solar flares are also associated with the coronal mass ejection, which can affect also Earth's magnetosphere and causes for example the auroras. Should a flare of high energy release occur on the Sun, it could also have a negative effect on the live on the Earth, for example in 1989 an outage of electricity transmission system in Québec was caused by an eruption on the Sun which resulted in coronal mass ejection.

Study of the stellar activity is also important for the study of the exoplanets, for which the habitability zone of their host stars can be affected by the activity, especially in case of red dwarfs and other active stars.

This diploma thesis presents the study of a low-mass eclipsing binary GJ 3236 based on spectroscopic and photometric data obtained during the years 2012 and 2018 at various observatories and using various photometric filters. The analysed photometric data consist of more than 80000 frames among which 241 flares have been detected. The binarity of the system allows determination of the parameters of both components based on spectroscopic and photometric data. For binaries, for which high-dispersion spectroscopy is available, the parameters can be derived with the accuracy about 1 %, which makes binary systems good candidates for testing of evolution models of the stars.

1. Theory

1.1 Binaries

Binaries are two stars, which are gravitationally bounded and orbit around mutual center of gravity. Binaries and multiple star systems are common, as was shown for example by Duchêne and Kraus (2013) and they even outnumber single stars.

Multiplicity of a system can be determined by three basic methods:

If the stars of a binary system can be resolved as two different light source, the system is called a visual binary and it is possible to directly observe the two stars orbiting around each other. Most of the binaries cant be resolved as two different light source and their multiplicity has to be determined by other means.

When two stars orbit around each other, their radial velocity differs during the orbit. The changes in radial velocity are periodical and can be determined from spectroscopic observations by measuring the shift of observed spectral lines. These system are called spectroscopic binaries.

If orbital plane of a binary system is almost parallel to the line-of-sight, then we can observe eclipses of the binary components. These systems are called Eclipsing binaries.

Study of eclipsing binaries' light curve and radial velocities can provide properties of the system such as mass, radius or luminosity of both components. Binaries are therefore good candidates for testing of stellar evolution models.

1.2 Red dwarfs

Red dwarfs are cool main sequence stars of mass between $0.08M_{\odot}$ and $0.5M_{\odot}$, spectral type of these stars is K and M (M-dwarfs). According to Henry et al. (2006), 72% of stars in Solar neighbourhood are red dwarf and also initial mass function presented by Kroupa et al. (2013) implies, that low-mass stars are the most common type of stars.

Red dwarfs have deep convective zones, which lead to creation of a chromosphere and a corona around these stars. If the mass of a star is smaller then $0.35M_{\odot}$, than the star is according to Chabrier and Baraffe (1997) fully convective. The existence of a chromosphere and a corona can be determined according to Harmanec and Brož (2011) for example by presence of emission lines of the Balmer series or CaII K and H emission lines. Radial velocities derived from lines originating in the chromosphere or the corona can differ from radial velocities derived from absorption lines originating in photosphere. Harmanec and Brož (2011) give as an example of this phenomenon the star α Ori, for which the Hα emission line is blue-shifted with respect to the photosphere.

Eclipsing binary systems consisting of two red dwarfs are called low-mass eclipsing binaries and according to Cruz et al. (2018) just a few tens of these systems are well-characterized. Low-mass eclipsing binaries are showing inconsistencies with the current stellar models, as the radii of the components derived from the light curve analysis are usually bigger by 5 % to 10 % than the radii predicted by stellar models. This phenomenon was addressed for example by Cruz et al. (2018) and yet remains to be solved.

1.3 Flare stars

Flare stars are variable stars for which phenomenon known as flare was observed. Flares are events of sudden brightening over a short amount of time, which is than followed by a slower decay, which can last for several tens of minutes. The star may brighten due to the flare as much as several magnitudes and the brightening can be observed on wavelengths ranging from X-ray to radio waves. An example of a light curve containing flares is shown in the Figure 1.1.

First flare stars were detected in the early 20th century, according to Joy (1967) the first observation of a flare was recorded by Ejnar Hertzsprung in 1924. A well studied flare star is UV Ceti, which also gave name to the UV Ceti class of eruptive variables in General Catalogue of Variable Stars[1]. Flares stars were associated mainly with the M dwarf stars, but as was shown on *Kepler* data by Balona (2015), flares can be observed for various spectral types ranging from M to A types, although the rate of observed flares decreases for stars of earlier spectral type, which might be just a selection effect. Properties of the flare stars of different spectral types were studied by Balona et al. (2016).

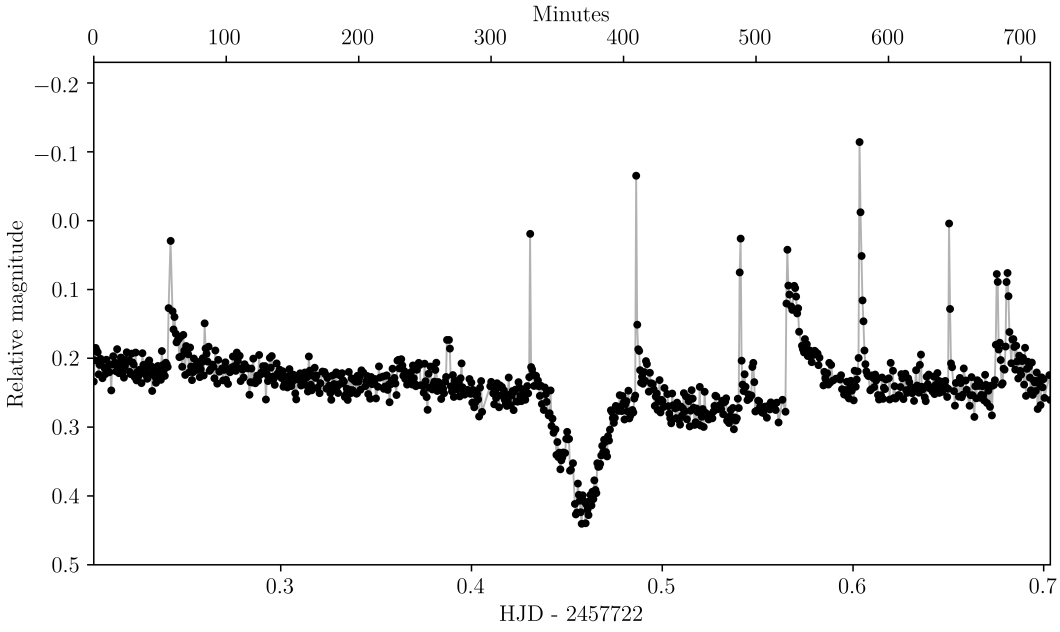

Figure 1.1: Light curve of GJ 3236 obtained in a B photometric filter at the Piszkéstetö Observatory on the 29th November 2016. Several flares have been detected during observation.

1.4 Stellar activity

Flares are explosive events connected with the magnetic activity of stars. They have been observed on stars of various type including the Sun. It is the high-resolution observations of the Solar eruptions which give us insight into the mechanism of the flare creation.

[1] `www.sai.msu.su/gcvs/gcvs`

Mechanism of eruptions

The standard model for describing solar flare mechanism is CSHKP (Carmichael-Sturrock-Hirayama-Kopp-Pneuman) model. The mechanism based on this model was described by Karlický (2014) as follows: A magnetic current-carrying loop is created between two polarities in an active region. Then the magnetic loop becomes unstable due to external perturbation or internal instabilities and starts to move upwards with its end still anchored to the dense layers of solar atmospheres. An enormous electric current flows through the magnetic loop, but because of its low current density does not dissipate. The situation below the rising loop is different and it allows the current sheet there to become sufficiently narrow and the current density sufficiently high for the magnetic reconnection to set in. This leads to the release of energy accumulated in the magnetic field in a form of accelerated particles and heating of the plasma.

The CSHKP model describing flare mechanism is two-dimensional and attempts to generalize the model in three dimensions have been made, for example by Aulanier et al. (2012).

Eruptions on the Sun and other stars

It is believed that flares observed on the Sun and flares observed on other stars are propelled by the same mechanism. Occurrence rate of flares $\frac{dN(E)}{dE}$ can be described as a function of energy E by the power law

$$\frac{dN(E)}{dE} \propto E^{\alpha}, \tag{1.1}$$

where $N(E)$ stands for the number of flares at a given energy E and α is the index of the power law, which is for solar flares $\alpha \approx -1.7$.

Superflares on solar-type stars were studied by Shibayama et al. (2013) and the energy distribution of superflares on these stars showed to follow a power law similar to the one describing energy distribution of solar flares, with $\alpha \approx -2$ for solar-type G stars. Comparison of the Occurrence rates presented by Shibayama et al. (2013) is shown in the Figure 1.2. Authors also showed, that superflares stars tend to have large stellar spots, whose sizes can be 10 times larger than the sizes of the largest sunspots.

Study of flares on stars of various spectral type was performed by Balona et al. (2016), who analysed roughly 3000 flares observed by the *Kepler* satellite in the short-cadence mode with exposure times of 1 min. The mean energy of the flares observed on A stars was 10^{29} J and for the F–M stars 10^{28} J. Indices of the power law describing the energy distribution for various type stars presented by Balona et al. (2016) are -1.65 for K–M stars, -1.70 for G stars, -1.56 for F stars and -1.34 for A stars. The same data set was also analysed by Švanda and Karlický (2016), who using different method determine the power indices to be $-1.79(6)$ for K stars, $-1.59(2)$ for G stars, $1.77(7)$ for F stars and $-1.37(7)$ for A stars.

Various models of flares assume, that the duration of a flare can be used as a reasonable estimate of the reconnection time τ_{rec} of the magnetic field, as was stated by Balona et al. (2016). The reconnection time can be estimated using the reconnection speed, which can be assumed to be approximately proportional

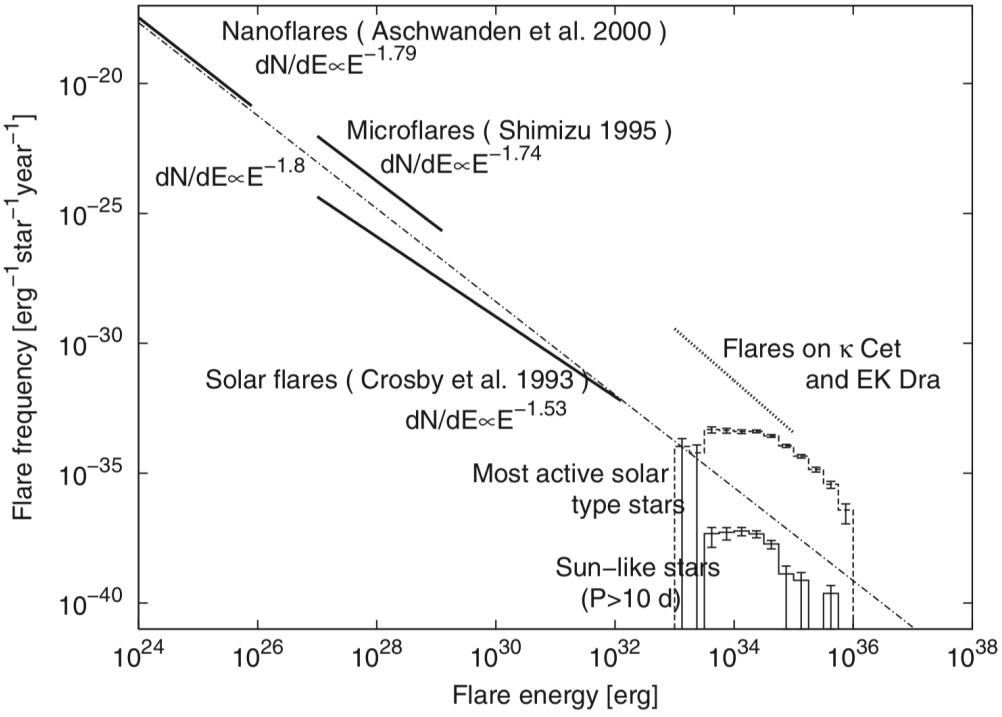

Figure 1.2: Occurrence rate of the superflares on G-type dwarfs and of the solar flares as presented by Shibayama et al. (2013). The solid-line histogram is showing energy distribution of solar-type stars, the dashed-line histogram represents energy distribution on the most active G-type dwarf stars. The solid lines represent power law distribution of solar flares derived from observation in various spectral range: EUV Aschwanden et al. (2000), soft X-rays Shimizu (1995), and hard X-rays Crosby et al. (1993). The dash-dotted line represents power law with $\alpha = -1.8$.

to the Alfvén speed v_A. The duration of a flare Δt can be than estimated as

$$\Delta t \sim \tau_{rec} \propto \frac{L}{v_A M_A}, \tag{1.2}$$

where L stands for the length-scale of the magnetic field and M_A is a non dimensional reconnection rate.

Assuming that the energy E released during a flare is proportional to the total magnetic energy of the dissipated magnetic field E_m, which can be estimated by

$$E_m \propto B^2 L^3, \tag{1.3}$$

where B stands for the average magnetic field. By combination of equation 1.2 and 1.3 and assuming that v_A, M_A and B are similar among stars of the same type, one can derive relation between flare duration and released energy

$$\Delta t \propto E^{\frac{1}{3}}. \tag{1.4}$$

Balona et al. (2016) tested the relation $\Delta t \propto E^{\beta}$ on flares of various spectral types and the derived β indices were close to the expected value of 1/3, for stars of spectral type K-M $\beta = 0.28(1)$ with correlation coefficient of 0.60. Visualisation

of the relation can be seen in the Figure 1.3, where data published by Balona (2015) were used. This data set contains 3140 flares observed on 209 stars of various type. Flares observed on the star KIC 2300039 are highlighted green to show an example of the dependency for a single star. As can be seen from the flares observed on this star, the β index can vary for individual stars, in this case $\beta = 0.69(4)$, which is approximately two times larger value than the one predicted by equation 1.4. The Table 1.1 contains β indices derived for stars of effective temperature smaller than 4000 K for which 10 or more flares are listed in data set published by Balona (2015), plot of the data is shown in the Figure 1.4. For these stars the β indices lie between values 0.34 and 0.74, but the analysis of the whole set gives $\beta = 0.32(2)$ with correlation coefficient 0.58.

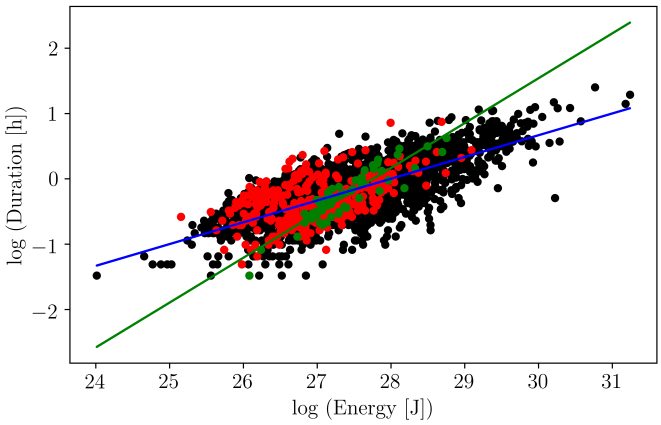

Figure 1.3: Relation between the released energy and flare duration for a set of 3140 flares. Red dots represent stars of effective temperature smaller than 4000 K (454 flares), green dots represent star KIC 2300039 (65 flares). Blue line represents expected dependency with $\beta = 1/3$, the green line represents linear fit of the KIC 2300039 data, for which $\beta = 0.69(4)$.

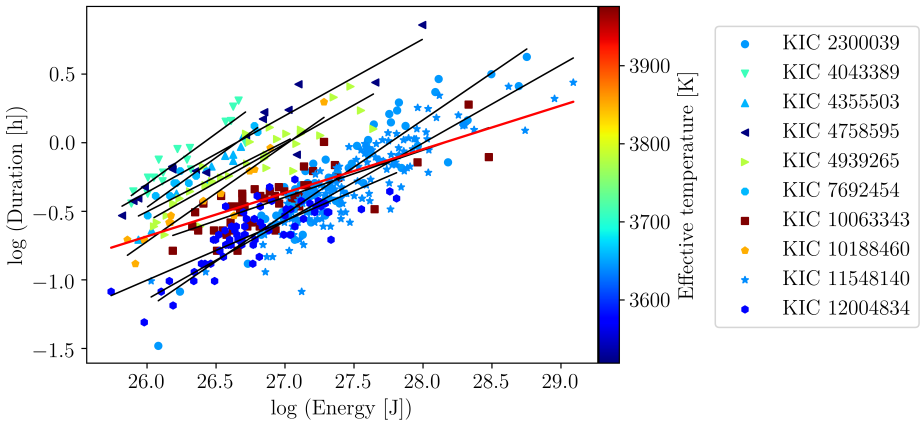

Figure 1.4: Relation between the released energy and flare duration for stars of effective temperature smaller than 4000 K presented by Balona (2015). Only data for stars for which 10 and more flares were observed are shown here. Black lines represent linear fits for individual stars, red line represent linear fit of the whole set with $\beta = 0.32(2)$.

Table 1.1: Indices of the relation of flare duration and released energy for stars with effective temperature smaller than 4000 K for which 10 and more flares have been observed. Based on the data published by Balona (2015).

KIC	β	Correlation coefficient	Flare count
2300039	0.69(4)	0.91	65
4043389	0.74(8)	0.91	17
4355503	0.51(19)	0.65	12
4758595	0.56(5)	0.95	16
4939265	0.57(5)	0.90	31
7692454	0.72(6)	0.97	10
10063343	0.34(4)	0.78	46
10188460	0.71(7)	0.95	13
11548140	0.57(3)	0.87	159
12004834	0.43(4)	0.79	69

1.5 GJ 3236

GJ 3236 is an eclipsing binary star consisting of two red dwarf stars. Its properties are listed in the Table 1.2. The binary was first observed in the constellation Cassiopeia, near the border with constellation Camelopardalis. Because of its high proper motion, it is moving towards the constellation Camelopardalis, in which it is currently situated. As an another consequence of the high proper motion ($\mu = 196.5(1)$ mas/yr), the binary GJ 3236 is moving towards a fainter star, with which it is currently overlapping, as can be seen of the Figure 1.5 and which could be problematic for magnitudes derived by aperture photometry. Thanks to its high declination, this star is suitable for observation from Czech Republic and long time series can be made during a night.

The star was listed in the catalogue of the flare stars located in the solar vicinity by Gershberg et al. (1999) and was classified as a spectroscopic binary by Pourbaix et al. (2004). First detection of eclipses of this binary system was reported by Irwin et al. (2009), who also derived its properties based on spectroscopic and photometric observations. In the light curve assembled from observations in V photometric filter a flare is present shortly after secondary minimum (phase $\sim$ 0.55) of amplitude $\sim$ 0.04 magnitude and this flare is probably first one published.

The binary was subsequently studied by Parimucha et al. (2016), who performed analysis of newly obtained photometric data and also observed 7 flares. Paper by Šmelcer et al. (2017) concerns with the flare activity of this binary system based on 59 observed flares.

Rotational period of the binary system was derived by Newton et al. (2016) to be $P = 0.386$ days, which is roughly half of the orbital period and is probably incorrect. The rotational period was derived by analysis of the variations of the light curve caused by the stellar spots, which were observed by the MEarth project. Data from this project were also used for the detection of eclipses by Irwin et al., 2009 and the light curve presented by Irwin et al., 2009 shows two out-of-eclipse increases caused by stellar spots, which probably led to the determination

Table 1.2: Properties of eclipsing binary GJ 3236.

Property	Value
Other designations	SBC9 3008, 2MASS J03371407+6910498, Gaia DR2 494406712082475520, GSC 4327:640
Coordinates (J2000)[a]	03h 37m 14.08s, +69°10' 49.8"
Proper motion in right ascension[b]	156.82(5) mas/yr
Proper motion in declination[b]	−118.47(7) mas/yr
Radial velocity[c]	16.95(3.55) km/s
Parallax[b]	26.91(4) mas
Distance based on the parallax[b]	37.16(6) pc
Spectral type[c]	M3.8+M4.4
B magnitude[d]	15.723(17) mag
V magnitude[d]	14.202(13) mag
R magnitude[d]	13.991(100) mag
I magnitude[e]	10.91 mag

[a] Cutri et al. (2003)
[b] Gaia Collaboration (2018)
[c] Shkolnik et al. (2010)
[d] Zacharias et al. (2012)
[e] Monet et al. (2003)

of a rotational period of 0.386 days. Recent observations of GJ 3236 show only one out-of-eclipse increase of brightness which can be described by a single stellar spot and with a rotational period equal to the orbital period of the system, which is roughly 0.77 days.

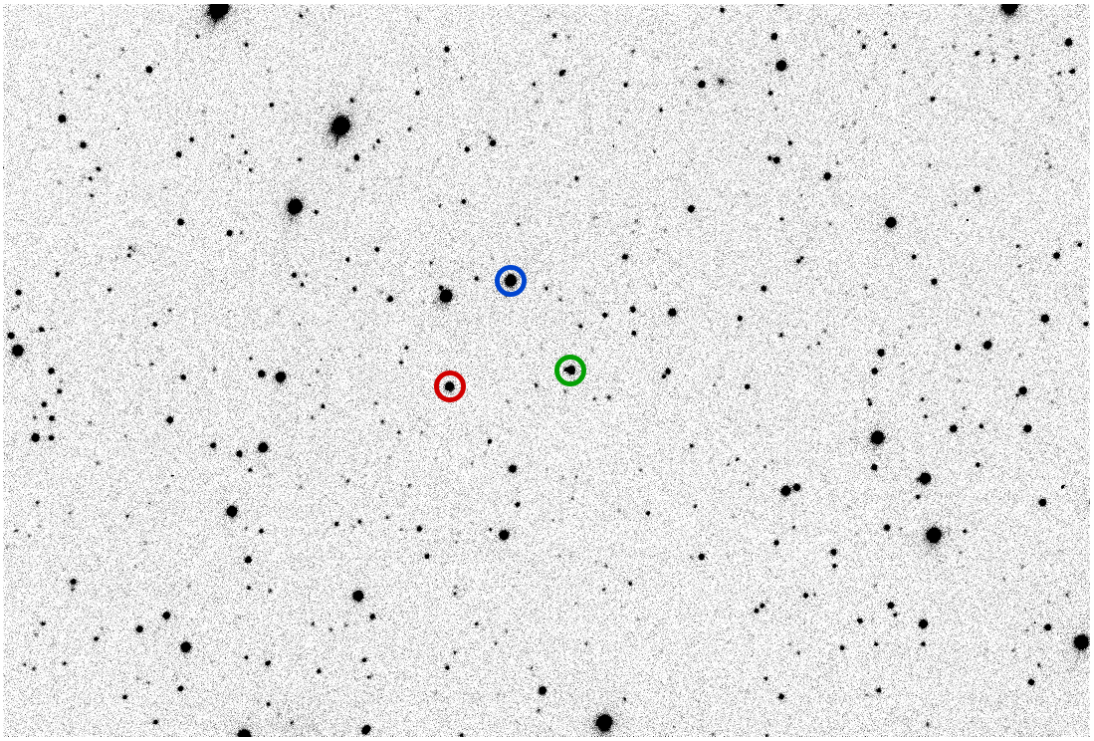

Figure 1.5: Image of the star field showing binary star GJ 3236 (green circle) obtained by the 65-cm telescope at the Ondřejov observatory on the 18th May 2017 with exposure time of 60 s. The red circle marks the star GSC 4327:2084, which was used as a comparison star for the aperture photometry analysis of the data obtained at the Ondřejov observatory, the blue circle marks the star GSC 4327:784, which was used as a check star. The field of view is roughly 20' × 14', north is up and east is left.

2. Spectroscopy

2.1 Spectroscopic data

Spectroscopic data were obtained at the San Pedro Mártir Observatory in Mexico with a 2.12-m telescope equipped with an echelle spectrograph, which is operated by National Autonomous University of Mexico. The spectrograph is capable of a resolution of R ∼18000 at wavelength of 500 nm and the spectra cover wavelengths from 360 nm up to 730 nm.

Observations took place during three nights in November 2016 and 14 spectra with exposure time of 20 minutes were obtained in total. Spectroscopic data were reduced using standard procedures in IRAF[1]. Figure 2.1 shows an example set of echelle orders obtained on the 18th November, defective measurements caused by cosmic radiation were removed. All echelle orders for the same observation are shown in Figures A.1, A.2 and A.3. The most prominent features of the spectra are Hα and Hβ emission lines of both components of the binary.

2.2 Radial velocities analysis

Radial velocity determination

Radial velocities were determined by fitting Hα lines, which is present in the spectra as two clearly separated peaks and is less affected by noise than Hβ line, which is also present in the data. Spectra containing Hα were normalized using IRAF function CONTINUUM and then sections between 6543 Å and 6581 Å were extracted to text file for further analysis.

Fitting of Hα lines was performed using programming language PYTHON3 and package LMFIT[2]. The shape of Hα line was modelled by two Voigt profiles and a continuum. Two examples of fitted lines are shown on Figure 2.2.

Radial velocities were computed from centers of fitted peaks using formula for Doppler shift

$$v = c\frac{\lambda - \lambda_0}{\lambda_0}, \tag{2.1}$$

where v stands for velocity, c stands for speed of light, λ stands for the shifted wavelength and λ_0 for the laboratory wavelength. Radial velocities were then corrected for the Heliocentric correction, which was calculated using program IRAF and its function RVCORRECT. Informations of observatory location and time of observation were taken from the header of the fits files of the spectra. Derived radial velocities are listed in Table 2.1.

Radial velocity curve

Previously published data by Irwin et al. (2009) were used for radial velocity analysis, namely, radial velocities derived by comparison with spectra of star GJ 856A, which were also based on Hα emission line. Radial velocities of the

[1] `iraf.noao.edu`

[2] `lmfit.github.io/lmfit-py`

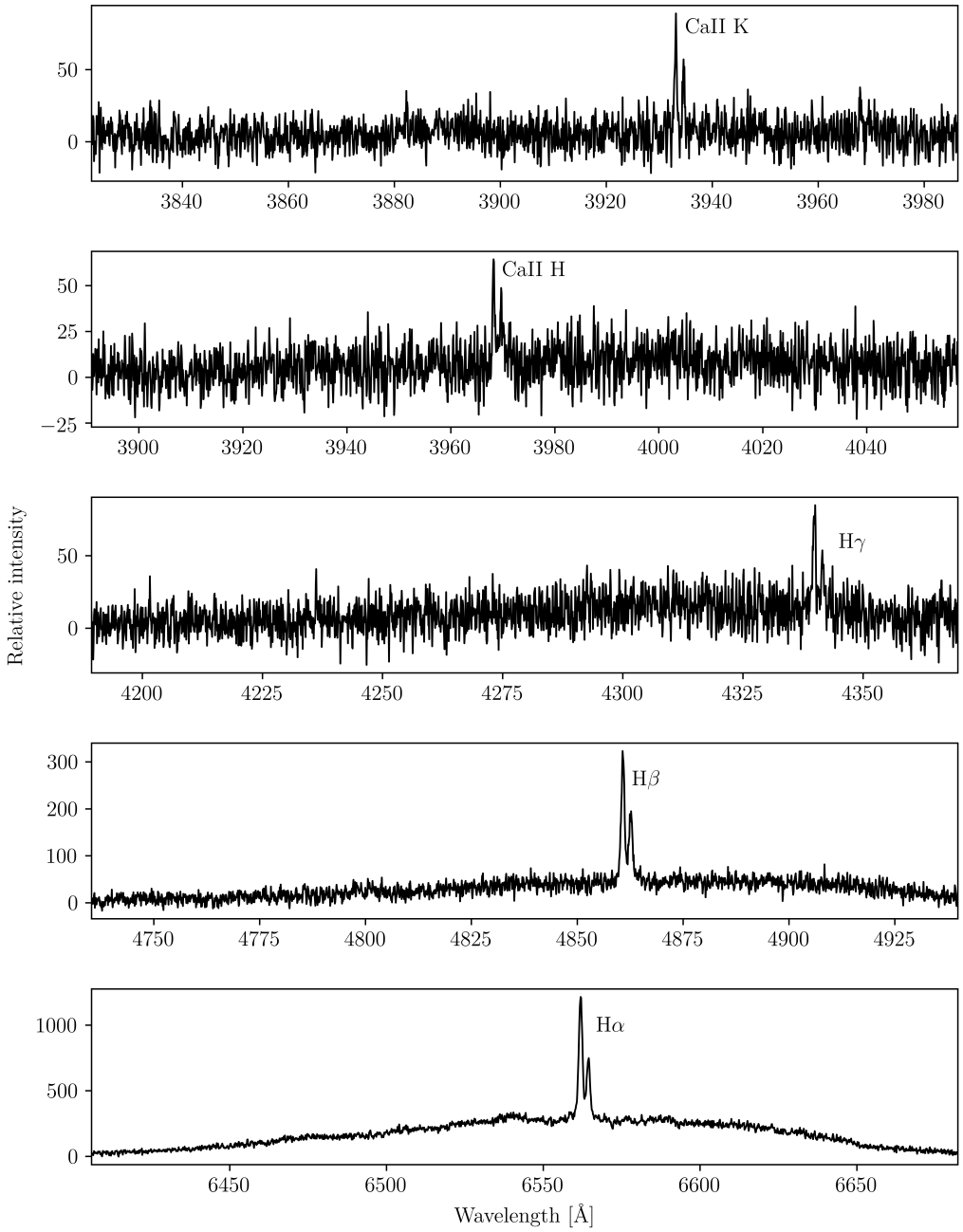

Figure 2.1: Spectrum of GJ 3236 taken on the 18th November 2016 depicting orders 4, 16, 22, 26 and 27 (from bottom to the top) of the echelle image, where emission lines Hα, Hβ, Hγ, CaII K and H are present.

Table 2.1: Heliocentric radial velocities of the primary component (v_1) and the secondary component (v_2). Listed errors are based only on the fitting error.

HJD − 2400000	v_1[km s^{-1}]	error [km s^{-1}]	v_2[km s^{-1}]	error [km s^{-1}]
57707.85313	57.64	0.56	-32.29	1.12
57707.86729	64.65	0.45	-46.50	0.93
57707.88142	72.31	0.45	-59.51	0.93
57707.89801	81.39	0.48	-65.15	0.88
57709.80131	-35.46	0.44	87.04	1.02
57709.81543	-44.08	0.52	90.52	1.00
57709.82955	-52.10	0.49	98.98	1.00
57709.84381	-58.26	0.54	109.88	1.16
57709.85805	-65.55	0.52	115.97	1.05
57709.87252	-69.72	0.46	120.14	0.94
57710.79411	-42.61	0.36	89.69	0.76
57710.80825	-35.16	0.31	79.42	0.63
57710.82238	-27.13	0.34	69.12	0.69
57710.83654	-16.22	0.55	56.50	1.16

primary component from both data sets were used to determine period using program PERIOD04[3].

Phase-folded radial velocities are shown in Figure 2.3. Velocities of both components were fitted simultaneously with the theoretical model. In view of the fact, that the eccentricity of the system is close to zero, radial velocities of both components were fitted by a sine function. Fitting was performed using PYTHON3 programming language and the package SYMFIT[4]. Parameters derived by fitting are listed in Table 2.2, where K_1 and K_2 stand for the radial velocity amplitude of the primary and the secondary component, γ stands for the radial velocity of the binary system a q stands for the mass ratio of the binary system, which was derived from the radial velocity amplitudes. The γ velocities may be affected by the fact, that Hα emission line originates in the chromosphere and may be shifted with respect to the lines originating in the photosphere. This shows to be the case for this binary, as in paper by Irwin et al. (2009) the γ velocities of the system derived from Hα emission line are ~ 3 km s^{-1} larger than the one derived from absorption lines.

[3] www.univie.ac.at/tops/Period04

[4] pythonhosted.org/symfit

Table 2.2: Parameters derived from RV fitting

Parameter	Value
Period	0.77125419(90) days[a]
K_1	88.02(47) km s^{-1}
K_2	113.93(68) km s^{-1}
γ	13.60(28) km s^{-1}
$q = \frac{M_1}{M_2}$	0.773(6)

[a] Period was derived by PERIOD04 and during radial velocities fitting was kept as constant.

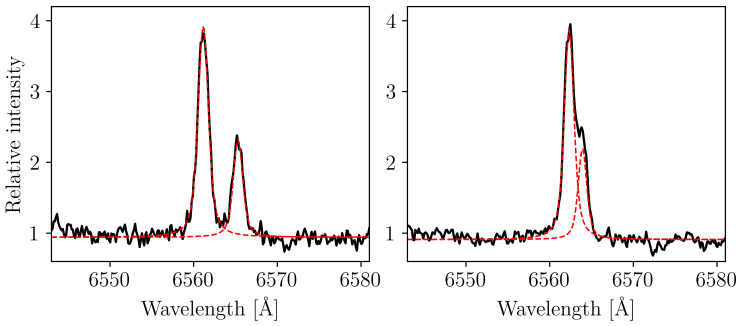

Figure 2.2: Fitting of Hα line for cases of highest and smallest separation of the two peaks. Black line represent measured data and red dashed lines represent separate fitted profiles consisting of Voigt profile and continuum. Left panel shows Hα line for phase 0.18, right panel depicts phase 0.43.

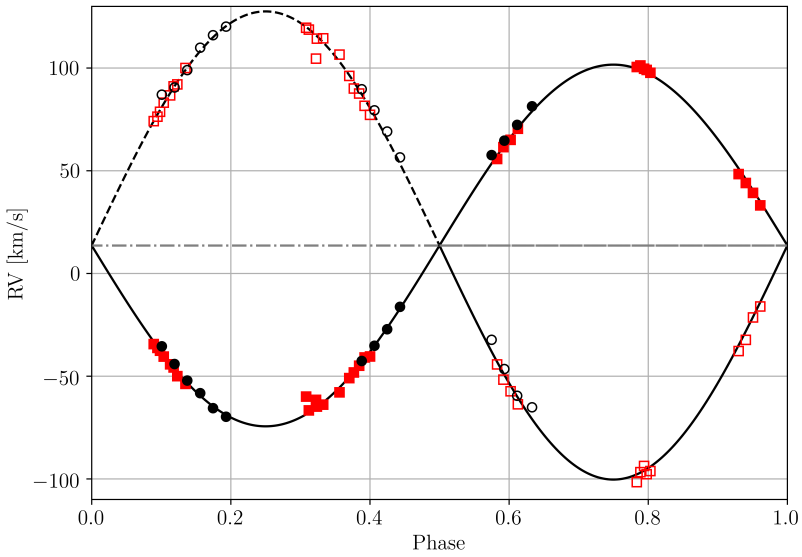

Figure 2.3: Phase-folded radial velocities for GJ 3236 system. Red squares represent data published by Irwin et al. (2009), black circles represent data from table 2.1. Filled symbols stand for the primary component and empty symbols stand for the secondary component. Error-bars would be smaller than the symbols. Velocities were phase-folded with a period of 0.77125419 days.

3. Photometry

3.1 Photometric data

Photometric data were acquired from five different observing sites. List of observations for all observation sites can be found in the attachments in Tables B.1 – B.11. For the monitoring of the flare activity only observation obtained before the 22nd February 2018 were taken in account. Light curves were obtained using aperture photometry.

Ondřejov

Photometric data at the Ondřejov observatory (Czech Republic) were obtained with a 65-cm telescope equipped with a G2-3200 CCD camera. Observations between the 13th September 2012 and 16th November 2015 were made with Johnson's R photometric filter, for subsequent observation Johnsons's V photometric filter was used, because the flares proved to be more prominent in the V filter. During years 2012–2015 mostly observations of minima were obtained. Observations in years 2016 and 2017 were more frequent and covered the light curve during all parts of phase. Photometric data were reduced by program Aphot32 developed at the Ondřejov observatory and also by C-MUNIPACK software[1]. As the star GJ 3236 is located in the obtained frames in proximity of another, fainter star, the aperture used in the Aphot32 program for aperture photometry was chosen to be 7×7 pixels large, so it would contain only the GJ 3236. Observations were carried out by Hana Kučáková, Kateřina Hoňková, Jan Vraštil, Kamil Hornoch and Marek Wolf.

Valašské Meziříčí

At the Valašské Meziříčí observatory (Czech Republic) a 25-cm telescope equipped with a G2-402 CCD camera and a Johnson's R photometric filter was used for obtaining of the photometric data. Observations took place between the 20th March 2014 and 31st August 2016. Additional observations with a Johnson's V photometric filter and with no filter were also obtained. Observations with the V filter were made in 2016 using a 35-cm telescope equipped with a G2-1600 CCD camera. Observation without any filter were obtained in 2017 using 28-cm telescope equipped with a G2-4000 CCD camera. Photometric data were reduced with C-MUNIPACK software. Observations were carried out by Ladislav Šmelcer. Flares present in the measurements obtained with R filter were already analysed by Šmelcer et al. (2017).

Trhové Sviny

Observations at the Trhové Sviny (Czech Republic) Observatory were obtained by 20-cm telescope equipped with an Atik 314L+ CCD camera. Observations were obtained using no filter and cover time between the 27th December 2015

[1] `c-munipack.sourceforge.net`

and 25th December 2017. Photometric data were reduced with C-MUNIPACK software. Observations were carried out by František Bílek.

Kolonické sedlo

Data from Kolonické sedlo observatory (Slovak Republic) were obtained with a 36-cm telescope equipped with a G2-1600 CCD camera, R, V and I photometric filters were used. Reduction of the photometric data was done using C-MUNIPACK software. These data were already analysed by Parimucha et al. (2016). Observations were carried out by Pavol Dubovský.

Piszkéstetö

Observation at the Piszkéstetö observatory (Hungary) were carried out using a 1-m telescope and took place during three nights in November 2016 and during two nights in January 2017. Johnson's B photometric filter was used for the observations and photometric data were reduced with C-MUNIPACK software. Observations were carried out by Marek Skarka.

3.2 Light curve analysis

For the light-curve analysis the program PHOEBE[2] was used, which is based on the standard Wilson and Devinney (1971) code. Detached binary model was used for the fitting.

For the light curve analysis data obtained between 14th September 2016 and 29th November 2016 were used. We have chosen data obtained during a short time span, so we would minimize any changes of the light curves shape caused by the variability of the spots on the components. Another criterion was to have even coverage of the light curve during its phase. Measurements obtained during the flares were removed from the data for the light curve analysis. For the photometric light curve sigma value 0.02 was chosen and for radial velocities curves sigma value 0.14 was chosen.

Parameters given by Irwin et al. (2009) were chosen as the initial parameters for the analysis, with exception of the period, the mass ratio and the radial velocity of the system, which we determined by the radial velocities analysis. Time of beginning of the phase $HJD0$ was chosen as the time of the primary minimum observed on the 14th September 2016, which was derived by fitting the minimum with a polynomial of the 6th order. The best fit of the light curve is shown in Figure 3.1, parameters of the best fit are listed in Table 3.1. The cost function value of the best fit is 135265.735025 for simultaneous fitting of the radial velocities and the light curve and the value for fitting solely the light curve is 495.753536. Figures 3.2 and 3.3 show mesh plots of the PHOEBE model of the binary system.

[2] `github.com/phoebe-project`, version from the 8th July 2012

3.2.1 Stellar spots

The brightness of binary GJ 3236 varies also outside the eclipses, as can be seen in the Figure 3.1. This variation has amplitude of approximately 0.06 magnitude in V filter with the maximal brightness at phase ~ 0.15. This variation is probably caused by spots on the components. In order to reproduce this out-of-eclipse variation, spots have to be introduced into the model. We have chosen a single large spot on the equator of the primary component (see Table 3.1), which has proved to be sufficient for reproduction of the variation. The spot is described by its latitude Θ_s, longitude Φ_s, radius r_s given in degrees and temperature ratio T_{spot}/T_p, which describes the ratio of the spot temperature and effective temperature the spotless primary component and we presume, that these parameters were constant for all observations included in the light-curve analysis. Visualisation of the location and the size of the spot can be seen in the Figure 3.2.

The shape of the light curve presented in this thesis is different, that the shape of light curves presented by Irwin et al. (2009) and Parimucha et al. (2016). Out-of-eclipse variation presented by Irwin et al. (2009) has amplitude of approximately 0.03 magnitude in V filter, which is half of the amplitude presented in this thesis. During one period of the binary, two out-of-eclipse brightening were present in the light curve, one with maximum at phase ~ 0.75 and the other at phase ~ 0.25. The second one had also smaller amplitude than the first one. Light curve presented by Parimucha et al. (2016) has out-of-eclipse variation with maximal brightness at phase ~ 0.25 and another small increase of brightness at phase ~ 0.7.

Residuals of the model fitting in figure 3.1 show, that apart from measurements during minima, the shape of the light curve is sufficiently fitted by one brightening and the residuals for out-of-eclipse measurements are best fitted with a constant function. It does not however prove the existence of a spot with given parameters, as the shape of out-of-eclipse variations could be also well fitted with spots situated on the secondary component or a group of smaller spots.

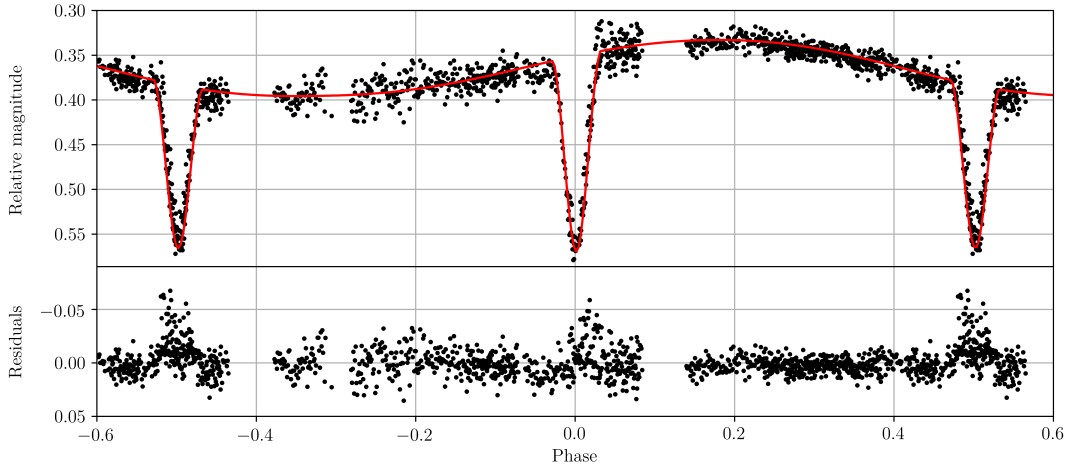

Figure 3.1: Phase-folded light curve in the V photometric filter. Relative magnitude is shown on the vertical axis of the top panel, red line represent best model obtained with the program PHOEBE. Bottom panel shows residuals of the fit.

Table 3.1: Parameters of best fit for the light curve analysis

Parameter	Value
$HJD0$	2457646.486968(200)
P	0.7712561264(5000) days
a	3.05(5) $R_\odot$
$q = \frac{M_1}{M_2}$	0.76997(1000)
γ^a	13.60(28) km s^{-1}
I	83.105°(20)
T_p	3241(200) K
T_s	3180(200) K
Ω_1	8.97477(15000)
Ω_2	8.88624(15000)
M_1	0.36(2) $M_\odot$
M_2	0.28(2) $M_\odot$
R_1	0.37(3) $R_\odot$
R_2	0.30(2) $R_\odot$
$M_{bol,1}$	9.39(23) mag
$M_{bol,2}$	9.92(23) mag
Spot:	
Component	Primary
Θ_s	90°(20)
Φ_s	299°(5)
r_s	87°(5)
T_{spot}/T_p	1.0123(10)

[a] γ velocity was kept constant during fitting and given value and error are based on the radial velocity analysis.

3.3 O-C diagram

An O-C diagram was constructed for the binary system. Observed times of the minima were derived from measurements obtained at the observatories Ondřejov, Valašské Meziříčí, Trhové Sviny and the observations of the minima published by Irwin et al. (2009) were also included. The centers of the minima were derived by fitting a polynomial function of the 6th order to the light curve depicting the eclipse.

Primary minimum observed by Irwin et al. (2009) on the 25th September 2008 was chosen as the initial epoch, which corresponds to $HJD = 2454734.995569$. The O-C diagram is shown in the Figure 3.4, the diagram was plotted for period $P = 0.771256094471$ d, for which the O-C values of primary minima are best fitted by a constant function.

A delaying of observation times for the secondary minima was recorded, as can be seen in the Figure 3.4. This delay ΔP can be described by a linear function of $\Delta P = 0.15(4)E$, where E stands for the epoch and the delay ΔP is given in seconds. The delay could be caused by stellar spots or other variances of the surface brightness of both components, which could change the shape of the light curve during the eclipses.

Figure 3.2: Mesh plot of the binary system model computed by PHOEBE for phase 0.25. Primary component is on the left side of the figure, the dark region represents position and size of the stellar spot used in the model.

Figure 3.3: Mesh plot of the binary system model computed by PHOEBE for phases 0.0 and 0.5. Primary component is the one with the dark region, which represents the position and the size of the stellar spot used in the model.

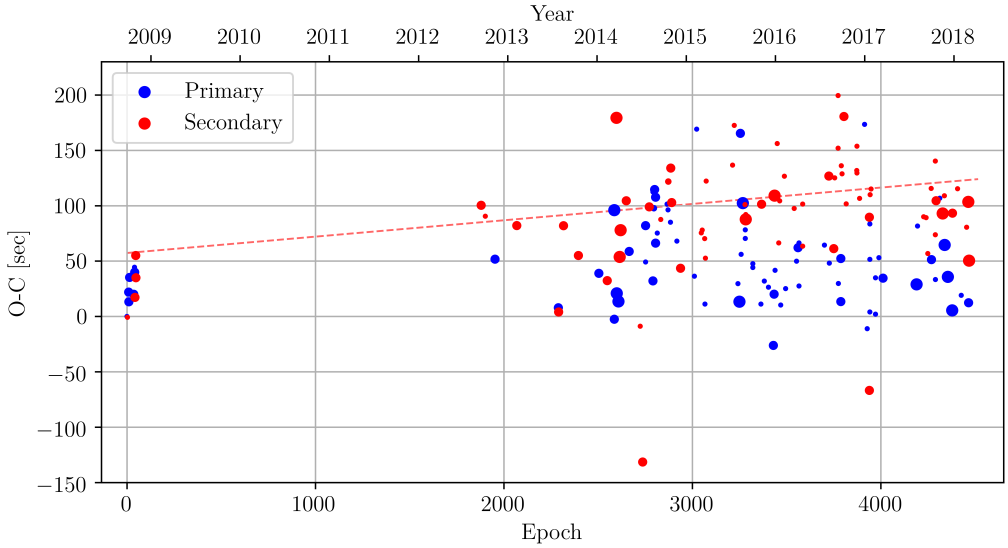

Figure 3.4: O-C diagram for primary and secondary minima of the binary GJ 3236. The size of the symbols correspond to the weight given to the individual measurements. The red dashed line represents linear fit of the O-C values for the secondary minima.

4. Flares

For flare activity analysis all data sets described in section 3.1 were used. A total of 241 flares were detected among the whole data set, all detected flares are listed in the Table C.12. Several examples of light curves containing flares are shown in the Figure 4.1.

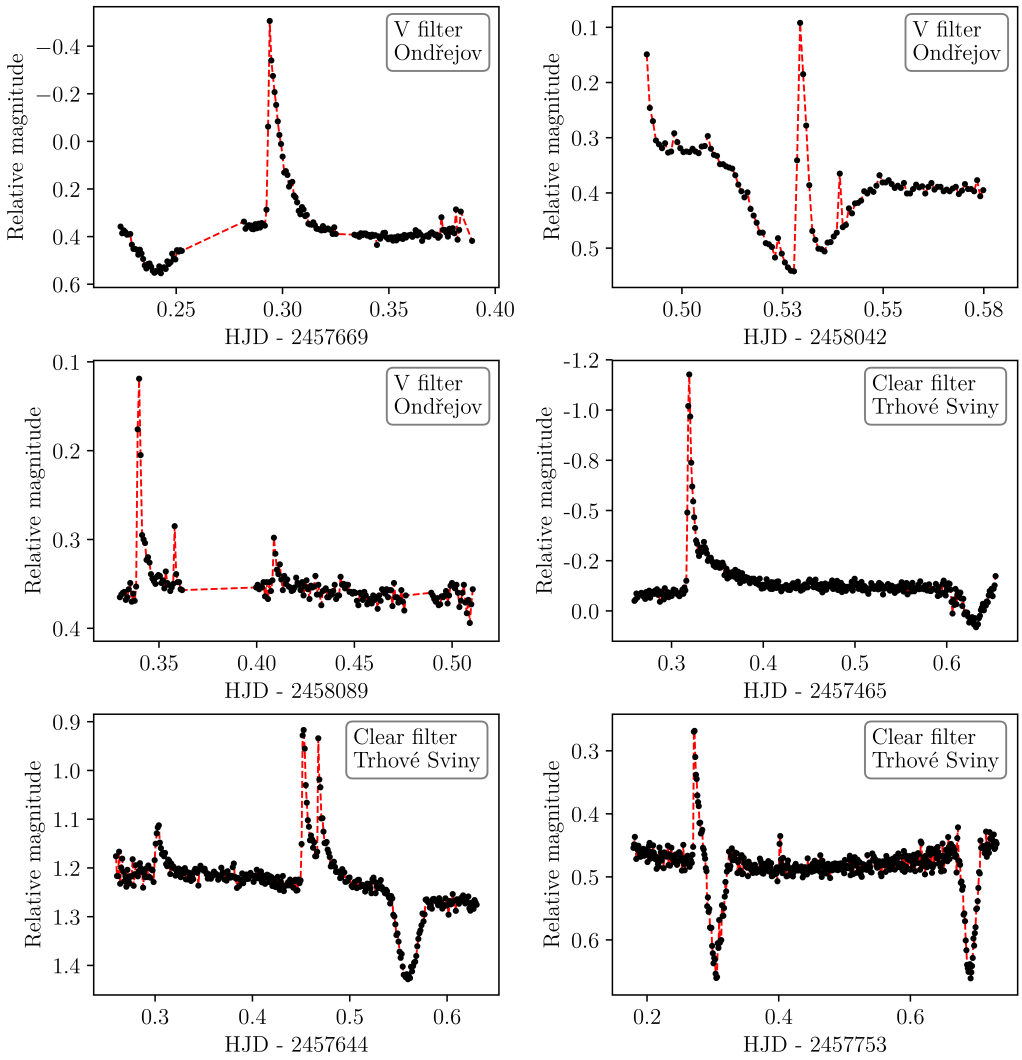

Figure 4.1: Examples of the light curves containing flares obtained at the Ondřejov observatory in filter V and at the Trhové Sviny observatory with clear filter. Scales of the axes vary for each light curve.

Comparison of observations in different photometric filters can be seen in the Figure 4.2, where the light curves of GJ 3236 obtained on the 29th November 2016 are shown. This comparison shows, that flares are more prominent when observed in the B filter. Even flares of amplitude ≈ 0.2 magnitude in B filter, which is similar to the depth of the minima in this filter, have amplitudes on other photometric filters comparable with the noise in the data and are therefore undetectable. This is caused by the decreasing brightness of the binary for used photometric filters centered on the shorter wavelengths, which make flares more

prominent. By this reasoning the flares should be also more prominent in the V filter with respect to the R filter, which shows to be true, as can be seen in the Table 4.1, where rates of flares for different photometric filter are computed. The rate of flares observed in the filter R at the Ondřejov Observatory is affected by the fact, that those observations contains mainly eclipses of the system, during which more flares are likely to be detected, as is further discussed in section 4.2.1.

Table 4.1: Rates of flares observed in various photometric filter.

Observatory & filter	Detected flares	Time observed [hours]	Rate [hours^{-1}]
Piszkéstetö B	41	31	1.32
Ondřejov V	44	149	0.28
Ondřejov R	7	29	0.24
Trhové Sviny C	111	642	0.17
Valašské Meziříčí R	52	795	0.07
Valašské Meziříčí C	5	33	0.15
Valašské Meziříčí V	6	25	0.24
Kolonické sedlo R	5	58	0.08
Kolonické sedlo V	3	19	0.16

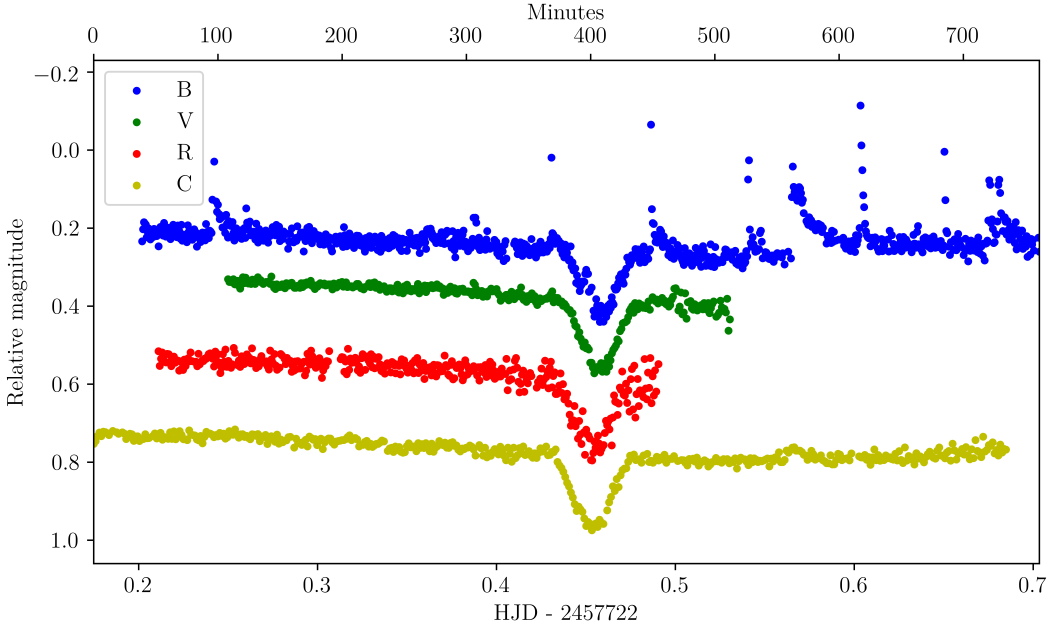

Figure 4.2: Comparison of light curves obtained simultaneously in different photometric filters on the 29th November 2016. Displayed light curves were obtained at the Piszkéstetö Observatory in filter B, Ondřejov Observatory in filter V and R and at the Trhové Sviny Observatory with clear filter. Light curve in the filter V was obtained using 65-cm telescope described in section 3.1, light curve in filter R was obtained by Martin Lehký using the BlueEye 60-cm telescope, data are available at the web site of the Variable Star and Exoplanet Section of Czech Astronomical Society, `var2.astro.cz/EN/obslog.php`.

4.1 Energy estimation

Luminosities of both components derived by the light curve analysis were used for the energy estimation of observed flares. The sum of out-of-eclipse luminosities of both components is $L_{1+2} = 0.0226\mathrm{L}_{\odot} = 8.65 \cdot 10^{24}\mathrm{W}$. Figure 4.3 shows a black-body radiation of a object with a temperature of the primary component and also amount of light observed in photometric filter B, V, R and I[1]. By integrating the curves we estimated the amount of total energy we observe in corresponding filter, which we then used to compute out-of-eclipse luminosities for each filter. This could not be done for observation with a clear filter, as these luminosities are defined by the quantum efficiency of the CCD camera, which were not available and therefore for flares observed in clear filters only relative energies were derived.

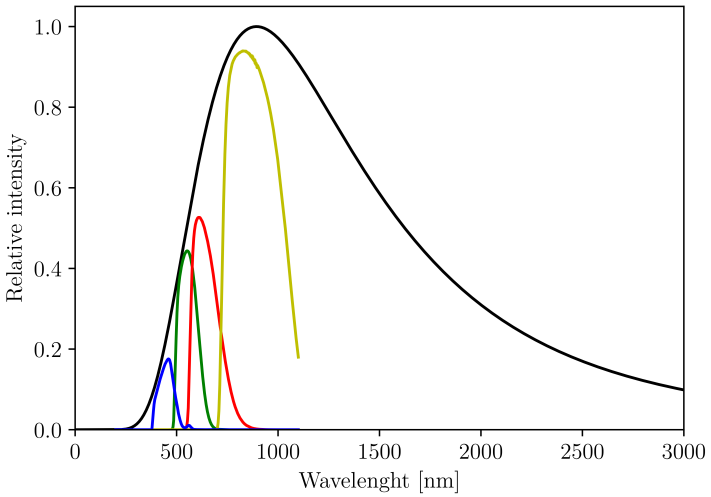

Figure 4.3: Black body spectrum for temperature T = 3241 K, red curve represents amount of the light observed with R filter a green curve represents amount of the light observed with V filter, blue line represents amount of the light observed in B filter and yellow line represents amount of the light observed in I filter.

We convert observed magnitude m_{obs} to luminosity L_{obs} by the Pogson's equation

$$L_{obs} = L_0 \cdot 10^{-0.4(m_{obs} - m_0)}, \tag{4.1}$$

where m_0 and L_0 stand for magnitude and luminosity for used photometric filter. Portion of released energy E recorded in the given filter can be calculated for flares out of eclipse by integration

$$E = \int_{t_1}^{t_2} L_0(10^{-0.4(m_{obs} - m_0)} - 1)\mathrm{d}t, \tag{4.2}$$

where t_1 and t_2 mark beginning and end of time when flare was observed. Integration was performed numerically on spline interpolation of the data using

[1]Filter curves were obtained from `www.aip.de/en/research/facilities/stella/instruments/data/johnson-ubvri-filter-curves`

Python3 package SciPy[2] and its functions interpolate.interp1d and integrate.simps.

Because of the out-of-eclipse variations in the brightness, an area defined by the spline function and a constant value was used for energy estimation. The constant value was determined by the last point of the light curve of a flare or the first point in cases, where the ending of the flare was not well covered. An example of the fitted curve and area used for the energy estimation is shown in the Figure 4.4. An example of the code used for the energy estimation is shown in the Section D.

This method of estimating released energy presumes, that the light curve of the observed flares is fully covered during the time of flare occurrence and that magnitude and therefore luminosity can be derived for each time by interpolation of the measured ones. Because of the need to read out the CCD chip, there is always a short interval of time, when the star is not observed. For observation at the Ondřejov Observatory the read-out time is typically 10 seconds. The energy released during a flare event could be then underestimated, should the maximal brightness coincide with the read out of the CCD chip.

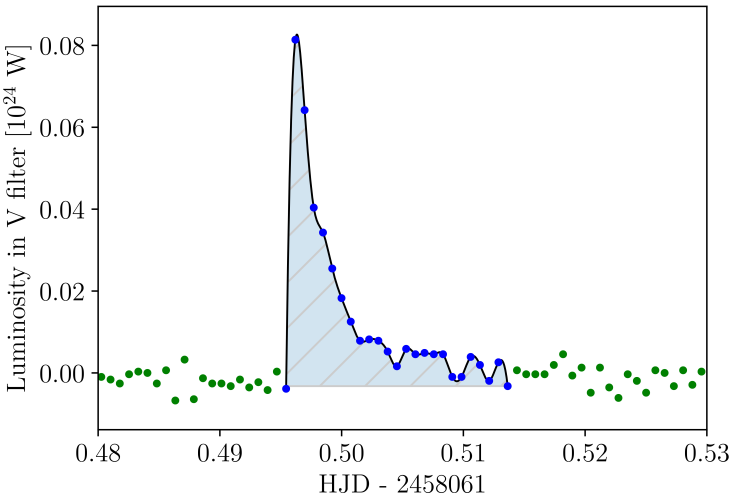

Figure 4.4: Light curve of a flare observed on the 3rd November 2017 fitted by a spline function. The area used for the energy estimation is highlighted blue.

4.2 Flare activity

4.2.1 Phase distribution

For the phase distribution analysis all observed flares were taken in account except for the flares observed at the Piszkéstetö Observatory, because these observations cover the phase unevenly. The histogram showing the distribution is shown in the Figure 4.5, where is also shown the histogram of all observation. As can be seen in that histogram, the system was observed more frequently during the eclipses, as these observation are essential for the O-C analysis. The histogram is showing

[2] `https://www.scipy.org`

distribution of observations of the system obtained at multiple observatories and some observations therefore corresponds to the same time.

The red-light histogram depicting rates was constructed by dividing the values of flare count by the values of frame counts and by adjusting the height, so that the highest peaks of rate and flare counts would have the same height.

There is a strong correlation between the relative magnitude of the system and number of observed flares in log-log space with correlation coefficient of 0.89. This is most likely caused by the fact, that flares are easier to detect when the star brightness is lower. Because of this fact, high amount of flares was detected during eclipses of the components. Another increase of flare occurrence happens after the secondary eclipse, when brightness of the system is decreased by the out-of-eclipse variations. The Figure 4.6 shows histograms of the flares observed at the Trhové Sviny Observatory sorted by their energies. For the estimation of the released energies of the flares observed during eclipses the first and last point of flares were used to determine the background luminosity. One can see that the flares of energies smaller than the median were observed mainly during eclipses and then in the second part of the phase, whereas the flares of energies larger than the median are distributed more evenly during the phase.

Apart from the increases of the flare occurrence caused by the changing brightness of the binary, an increase was detected also for the phase 0.2 which coincides with the maximal brightness of the system. This increase of the flare occurrence could be explained by an active region on a component, which could be responsible also for the brightening of the system seen in the light curve.

It is not possible to determine which component the observed flares originate from. Even during eclipses, when one component is blocked out by the other component, there is still a significant portion of the blocked out component visible, as can be seen in the Figure 3.3, where mesh plot of the system for phases 0.0 and 0.5 are shown.

4.2.2 Time distribution

For analysis of detected flares over time data sets of flares observed in the V filter at the Ondřejov Observatory and in the clear filter at the Trhové Sviny Observatory have been chosen, because these are the two largest sets apart from flares observed in R filter at the Valašské Meziříčí Observatory. Rate of flares of this data set is low, as can be seen in the Table 4.1 and is therefore not suitable for analysis of flare occurrence over time.

Distributions of flares observed at the Ondřejov Observatory and the Valašské Meziříčí Observatory and rates of flares are shown in the Figure 4.7, where histogram of observed time is also present. For both data sets an increase of rate was recorded in the second half of the year 2017. This period of time also coincide with an observation made at the Ondřejov Observatory on the 15th October 2017, when 6 flares were detected during 2 hours of observations, which is the highest amount of flares observed at that observatory during a single night. Light curve of this observation can be seen in the Figure 4.1 on the top-right panel. This may suggests that in the second half of the year 2017 the activity of GJ 3236 was increased.

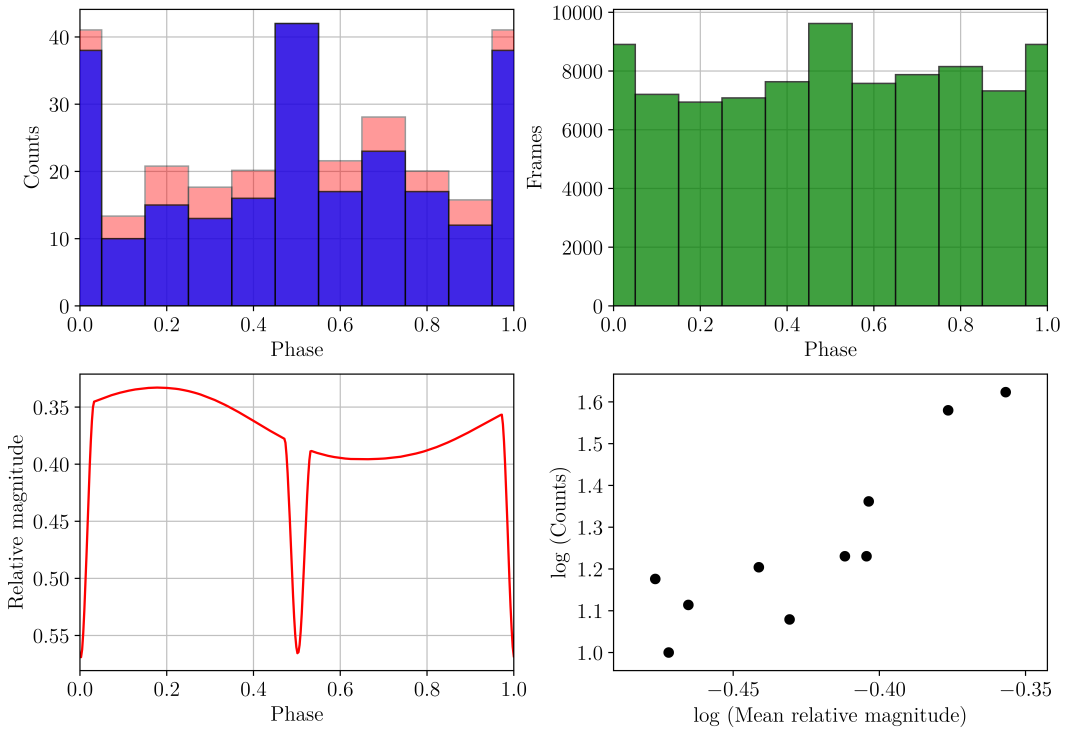

Figure 4.5: Histogram showing distribution of flares during phase (top-left). The blue histogram shows number of observed flares. The green histogram (top-right) shows distribution of all observations. The light-red histogram shows the rate of flares per frame, the values are normalised so the highest peaks of rate and counts would have the same height. The bottom-left panel shows the synthetic light curve of the binary system and bottom-right panel shows the correlation between relative magnitude of the system and the number of observed flares in log-log space.

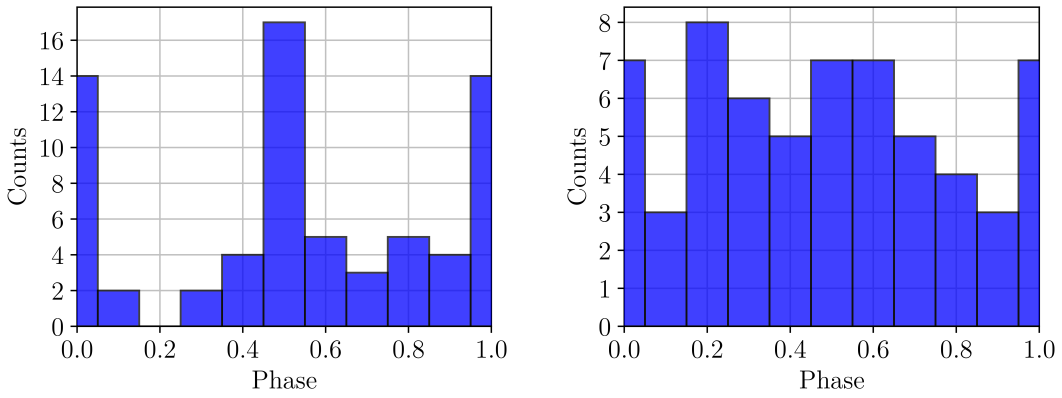

Figure 4.6: Histograms showing distribution of flares observed at the Trhové Sviny Observatory sorted by their energies. Left panel shows the flares of energies smaller than the median of the set, right panel shows the flares of energies larger than the median of the set.

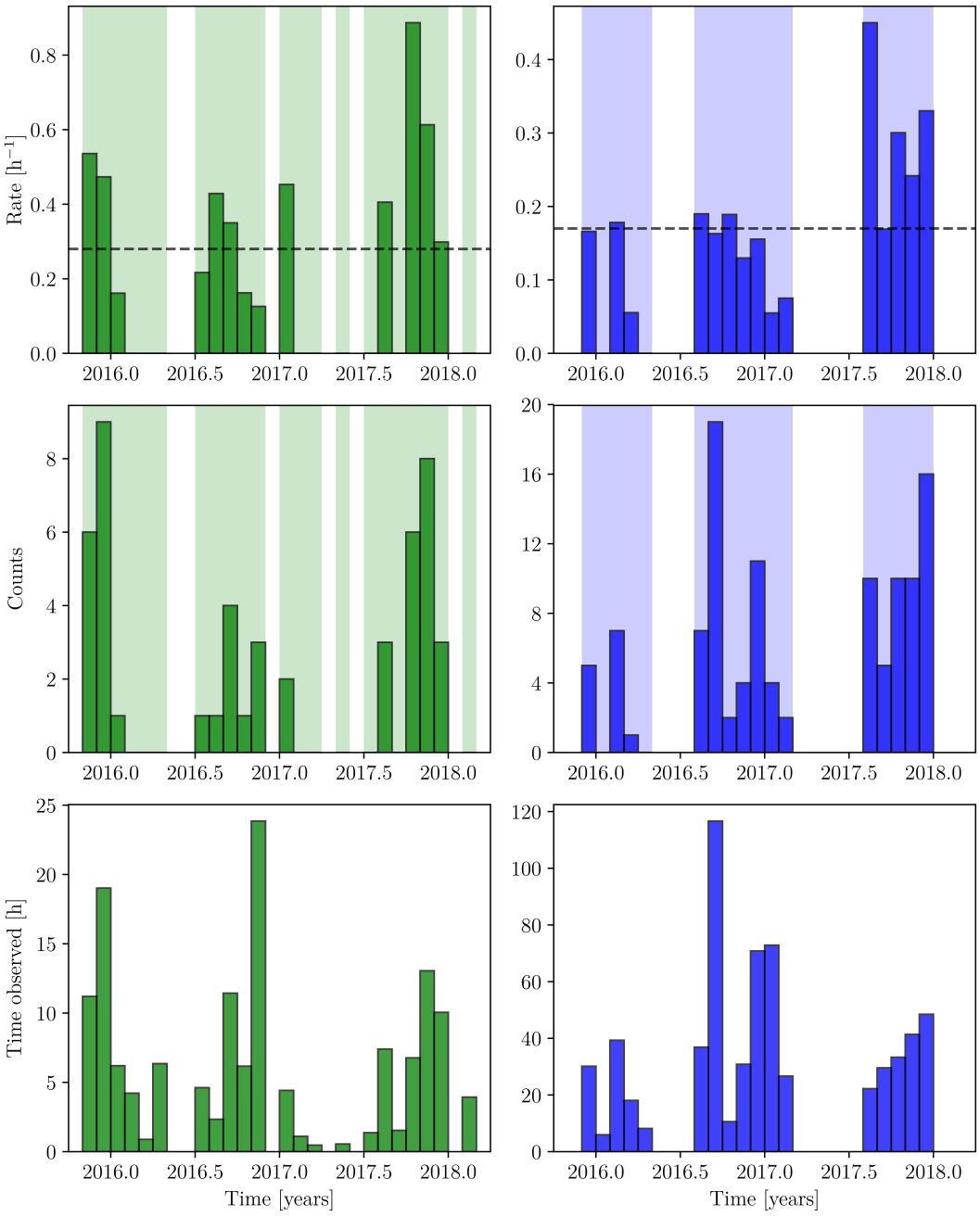

Figure 4.7: Histogram showing distribution of flare rates, flares and observation in time for observations obtained with a V filter at the Ondřejov Observatory (left panels) and for observations obtained with a clear filter at the Trhové Sviny Observatory (right panels). Filled areas represent months when the star GJ 3236 was observed, black dashed lines represent mean value of rates for given data set.

4.2.3 Energy distribution

For energy distribution analysis sets containing tens of flares were chosen. This includes flares observed at the Ondřejov Observatory in V filter, at the Valašské Meziříčí Observatory in R filter, at the Trhové Sviny Observatory and at he

Piszkéstetö Observatory. The histograms of energy distribution are in the Figure 4.8.

For estimation of the power law index the maximum likelihood method described by Bauke (2007) was used. This method is considered to provide better estimations for the power law parameters than the fitting of a linear function to histogram, which is highly dependable on the selection of the bins. Due to a selection bias caused by the detection limits of used equipment, there is decreasing number of flares for lower energies. Therefore the power law fitting was performed on the energies higher than a threshold energy, which was derived from the histograms. The threshold energies are listed in the Table 4.2 and are also marked in the histograms in the Figure 4.8. The derived indices of the power law for flares observed in various photometric filters are listed in the Table 4.2. The weighted mean of the power indices is $\alpha = 1.81(7)$, which is similar to the power indices of energy distribution of flares observed on other stars. This suggests, that the observed flares behaved similarly to the flares observed on other stars including the Sun and that the flares are powered by the same mechanism.

Table 4.2: Power law indices for flares observed in various photometric filters.

Observatory & filter	Detected flares	Threshold [10^{25} J]	α
Ondřejov V	44	0.40	$-1.87(20)$
Valašské Meziříčí R	52	0.70	$-1.69(11)$
Piszkéstetö B	41	0.23	$-2.23(29)$
Trhové Sviny C	111	11.26[a]	$-1.84(11)$

[a] Threshold energy for flares observed in clear filter is given in dimensionless value.

4.2.4 Flare duration

For flares, for which the released energy was estimated, the amplitude of the flare and the duration were also determined. Analysis of relations of the released energy, the flare amplitude and the flare duration was performed on the same data sets, which were chosen for the energy distribution analysis. The Figure 4.9 contains graphs showing relations between mentioned properties. Correlation coefficients and slopes of linear fits are listed in the Table 4.3. Out of the all considered relations, the one between amplitude and duration is the least correlated, with the average correlation coefficient of 0.51. The relations between the durations and the released energy and between amplitude and the released energy are highly correlated, with the average correlation coefficients 0.85 and 0.83 respectively.

The duration-energy relation can be described by equation $\Delta t \propto E^{\beta}$, as was mentioned in the section 1.4, where the β index corresponds to the slopes presented in the Table 4.3. The weighted average of β for all data sets is $\beta = 0.60(4)$, which is approximately two times larger value, then the one expected or the one derived by fitting data based on observation of multiple stars, but is in the range of β indices derived for individual stars presented in the Table 1.1.

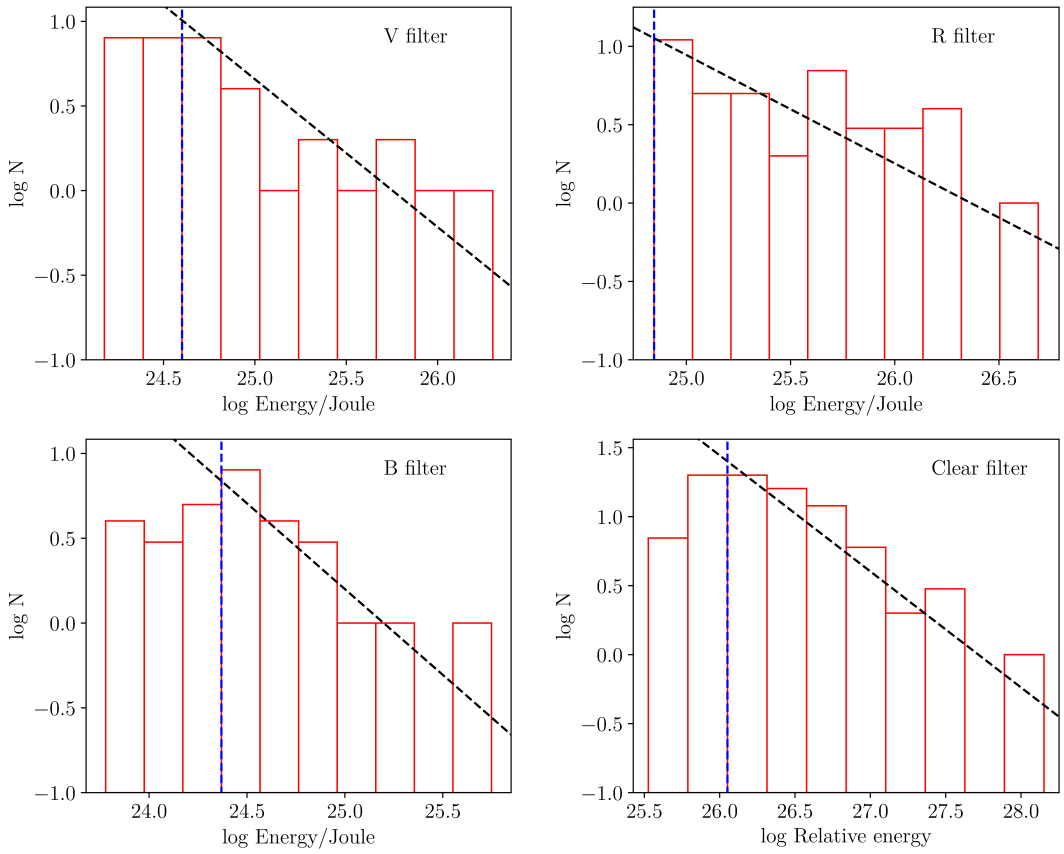

Figure 4.8: Energy distribution of flares observed in filter V, R, B, and clear filter. Black dashed line represents power law derived from given data set and blue dashed line represents threshold for the power law analysis.)

A study of flares observed on a M dwarf star GJ 1243 by Silverberg et al. (2016) shows a similar phenomenon of the amplitude-duration relation being less correlated then the duration-energy and amplitude-energy relations. The β index of the duration-energy relation for the star GJ 1243 was derived to be $\beta = 0.342(3)$.

Table 4.3: Relation between flares properties for various data sets. Correlations were computed for decadic logarithms of the quantities, slopes refers to the linear fits shown in the Figure 4.9.

Quantities	Correlation coefficient	Slope[a]
Ondřejov V		
Duration & energy	0.83	0.56(6)
Duration & amplitude	0.56	0.55(14)
Amplitude & energy	0.89	0.76(5)
Valašské Meziříčí R		
Duration & energy	0.83	0.57(6)
Duration & amplitude	0.46	0.43(13)
Amplitude & energy	0.84	0.61(6)
Piszkéstetö B		
Duration & energy	0.86	0.73(8)
Duration & amplitude	0.39	0.46(21)
Amplitude & energy	0.73	0.51(9)
Trhové Sviny C		
Duration & energy	0.88	0.64(4)
Duration & amplitude	0.61	0.68(10)
Amplitude & energy	0.86	0.56(4)

[a] Slopes are given for linear function, for which the dependent variable is shown in the Figure 4.9 on the vertical axis.

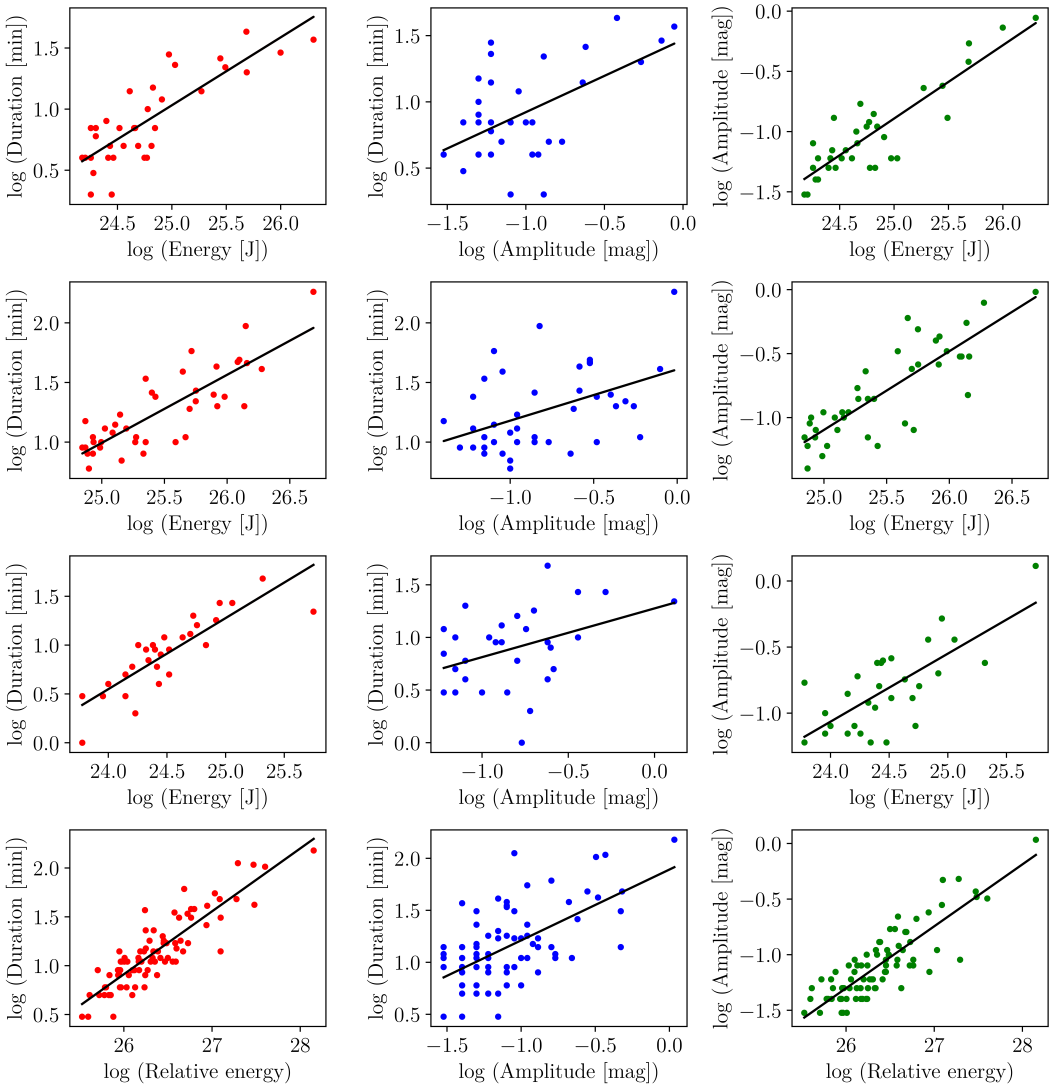

Figure 4.9: Graphs showing relations between flare duration, released energy and amplitude for filter V, R, B and clear filter (from top to bottom). Black lines represent linear fit of the data, slopes are listed in the Table 4.3.

Conclusions

Spectroscopic and photometric observations of the flare star GJ 3236 were obtained and precise physical parameters of this binary system were derived. The resulting parameters of the binary system derived are in agreement with previously published results by Irwin et al. (2009), however a change in out-of-eclipse variation caused probably by stellar spots has been recorded. This variations were fitted in the model by a single stellar spot. This solution is however not singular, as the variation can be fitted by other different configurations of spots. The change of the light curve shape suggest evolution of the stellar spots on the components. The light curve fit was performed on the data obtained in 2016, the light curve of the binary based on the data obtained in 2017 however shows the same out-of-eclipse variation only with smaller amplitude, which is approximately two thirds of the amplitude observed in 2016.

For the flare analysis photometric data obtained at the various observatories using various photometric filters were used, all photometric data consists of more than 80000 frames. A total of 241 flares were detected, which makes the presented data set the largest set of flares observed for this particular star. Sets of flares observed on the star GJ 3236 were previously published by Parimucha et al. (2016), who observed 7 flares and Šmelcer et al. (2017), who observed 59 flares.

The flare occurrence during phase was found to be correlated with the magnitude of the binary system, with highest flare occurrence happening during eclipses of the components. This can be explained by the fact, that flares are more easily detected for smaller brightness, as for this cases the brightening is more prominent. Another increase of the flare occurrence was detected for the phase 0.2 which coincides with the maximal brightness.

Time dependency of flare occurrence was analysed for two subsets of the observed flares and in both cases an increase of the activity was detected in the second half of the year 2017. This result is however based in both cases on a small sample of flares.

For flares observed out of eclipse released energies were estimated, which were in the range of 10^{24}–10^{26} J. For the flares observed in the clear filter only relative energies were derived. For four largest subsets of flares analysis of energy distribution was carried out. Indices of the power law distribution were derived for each subsets, the weighted mean value is $\alpha = 1.81(7)$ which is in agreement with the indices of other flare stars and also the Sun. This suggests, that the mechanism propelling the flares is the same as is for the Sun.

The relation between amplitude, duration and released energy of flares was analysed for four largest subsets of flares. For all subsets the amplitude-energy and duration-energy relation were highly correlated and the amplitude-duration was less correlated. The β indices of the duration-energy relation derived for GJ 3236 was for all four subsets of flares approximately two time larger than is the expected value. This inconsistency is however not unusual, as was shown on the case of stars observed by the Kepler satellite presented by Balona (2015), for which the β indices for stars of effective temperature smaller than 4000 K varies between values 0.34 and 0.74. This suggests, that the presumption which the relation 1.4 is based on were not fully met and that the relation can't be used

universally.

For more precise analysis of the stellar activity of the binary star GJ 3236 long observation series obtained using B photometric filter (or filter centered even on shorter wavelengths) would be very helpful, because observation in this filter have the highest flare rate and would therefore provide much larger set of flares than observations in other filters presented in this work.

Bibliography

Aschwanden, M. J., Tarbell, T. D., Nightingale, R. W., Schrijver, C. J., Title, A., Kankelborg, C. C., Martens, P., and Warren, H. P. (2000). Time Variability of the "Quiet" Sun Observed with TRACE. II. Physical Parameters, Temperature Evolution, and Energetics of Extreme-Ultraviolet Nanoflares. ApJ, 535:1047–1065.

Aulanier, G., Janvier, M., and Schmieder, B. (2012). The standard flare model in three dimensions. I. Strong-to-weak shear transition in post-flare loops. A&A, 543:A110.

Balona, L. A. (2015). Flare stars across the H-R diagram. MNRAS, 447:2714–2725.

Balona, L. A., Švanda, M., and Karlický, M. (2016). Differential rotation, flares and coronae in A to M stars. MNRAS, 463:1740–1750.

Bauke, H. (2007). Parameter estimation for power-law distributions by maximum likelihood methods. *European Physical Journal B*, 58:167–173.

Chabrier, G. and Baraffe, I. (1997). Structure and evolution of low-mass stars. A&A, 327:1039–1053.

Crosby, N. B., Aschwanden, M. J., and Dennis, B. R. (1993). Frequency distributions and correlations of solar X-ray flare parameters. Sol. Phys., 143:275–299.

Cruz, P., Diaz, M., Birkby, J., Barrado, D., Sipöcz, B., and Hodgkin, S. (2018). Low-mass eclipsing binaries in the WFCAM Transit Survey: the persistence of the M-dwarf radius inflation problem. MNRAS, 476:5253–5267.

Cutri, R. M., Skrutskie, M. F., van Dyk, S., Beichman, C. A., Carpenter, J. M., Chester, T., Cambresy, L., Evans, T., Fowler, J., Gizis, J., Howard, E., Huchra, J., Jarrett, T., Kopan, E. L., Kirkpatrick, J. D., Light, R. M., Marsh, K. A., McCallon, H., Schneider, S., Stiening, R., Sykes, M., Weinberg, M., Wheaton, W. A., Wheelock, S., and Zacarias, N. (2003). VizieR Online Data Catalog: 2MASS All-Sky Catalog of Point Sources (Cutri+ 2003). *VizieR Online Data Catalog*.

Duchêne, G. and Kraus, A. (2013). Stellar Multiplicity. ARA&A, 51:269–310.

Gaia Collaboration (2018). VizieR Online Data Catalog: Gaia DR2 (Gaia Collaboration, 2018). *VizieR Online Data Catalog*, 1345.

Gershberg, R. E., Katsova, M. M., Lovkaya, M. N., Terebizh, A. V., and Shakhovskaya, N. I. (1999). Catalogue and bibliography of the UV Cet-type flare stars and related objects in the solar vicinity. A&AS, 139:555–558.

Harmanec, P. and Brož, M. (2011). *Stavba a vývoj hvězd*. MatfyzPress, Prague.

Henry, T. J., Jao, W.-C., Subasavage, J. P., Beaulieu, T. D., Ianna, P. A., Costa, E., and Méndez, R. A. (2006). The Solar Neighborhood. XVII. Parallax Results from the CTIOPI 0.9 m Program: 20 New Members of the RECONS 10 Parsec Sample. AJ, 132:2360–2371.

Irwin, J., Charbonneau, D., Berta, Z. K., Quinn, S. N., Latham, D. W., Torres, G., Blake, C. H., Burke, C. J., Esquerdo, G. A., Fürész, G., Mink, D. J., Nutzman, P., Szentgyorgyi, A. H., Calkins, M. L., Falco, E. E., Bloom, J. S., and Starr, D. L. (2009). GJ 3236: A New Bright, Very Low Mass Eclipsing Binary System Discovered by the MEARTH Observatory. ApJ, 701:1436–1449.

Joy, A. H. (1967). Stellar Flares. *Leaflet of the Astronomical Society of the Pacific*, 10:41–48.

Karlický, M. (2014). *Plasma astrophysics*. MatfyzPress, Prague.

Kroupa, P., Weidner, C., Pflamm-Altenburg, J., Thies, I., Dabringhausen, J., Marks, M., and Maschberger, T. (2013). *The Stellar and Sub-Stellar Initial Mass Function of Simple and Composite Populations*, page 115.

Monet, D. G., Levine, S. E., Canzian, B., Ables, H. D., Bird, A. R., Dahn, C. C., Guetter, H. H., Harris, H. C., Henden, A. A., Leggett, S. K., Levison, H. F., Luginbuhl, C. B., Martini, J., Monet, A. K. B., Munn, J. A., Pier, J. R., Rhodes, A. R., Riepe, B., Sell, S., Stone, R. C., Vrba, F. J., Walker, R. L., Westerhout, G., Brucato, R. J., Reid, I. N., Schoening, W., Hartley, M., Read, M. A., and Tritton, S. B. (2003). The USNO-B Catalog. AJ, 125:984–993.

Newton, E. R., Irwin, J., Charbonneau, D., Berta-Thompson, Z. K., Dittmann, J. A., and West, A. A. (2016). The Rotation and Galactic Kinematics of Mid M Dwarfs in the Solar Neighborhood. ApJ, 821.

Parimucha, Š., Dubovský, P., Vaňko, M., and Čokina, M. (2016). Optical flare activity in the low-mass eclipsing binary GJ 3236. Ap&SS, 361:302.

Pourbaix, D., Tokovinin, A. A., Batten, A. H., Fekel, F. C., Hartkopf, W. I., Levato, H., Morrell, N. I., Torres, G., and Udry, S. (2004). S$_{B⁹}$: The ninth catalogue of spectroscopic binary orbits. A&A, 424:727–732.

Shibayama, T., Maehara, H., Notsu, S., Notsu, Y., Nagao, T., Honda, S., Ishii, T. T., Nogami, D., and Shibata, K. (2013). Superflares on Solar-type Stars Observed with Kepler. I. Statistical Properties of Superflares. ApJS, 209:5.

Shimizu, T. (1995). Energetics and Occurrence Rate of Active-Region Transient Brightenings and Implications for the Heating of the Active-Region Corona. PASJ, 47:251–263.

Shkolnik, E. L., Hebb, L., Liu, M. C., Reid, I. N., and Collier Cameron, A. (2010). Thirty New Low-mass Spectroscopic Binaries. ApJ, 716:1522–1530.

Silverberg, S. M., Kowalski, A. F., Davenport, J. R. A., Wisniewski, J. P., Hawley, S. L., and Hilton, E. J. (2016). Kepler Flares. IV. A Comprehensive Analysis of the Activity of the dM4e Star GJ 1243. ApJ, 829:129.

Šmelcer, L., Wolf, M., Kučáková, H., Bílek, F., Dubovský, P., Hoňková, K., and Vraštil, J. (2017). Flare activity on low-mass eclipsing binary GJ 3236*. MNRAS, 466:2542–2546.

Švanda, M. and Karlický, M. (2016). Flares on A-type Stars: Evidence for Heating of Solar Corona by Nanoflares? ApJ, 831:9.

Wilson, R. E. and Devinney, E. J. (1971). Realization of Accurate Close-Binary Light Curves: Application to MR Cygni. ApJ, 166:605.

Zacharias, N., Finch, C. T., Girard, T. M., Henden, A., Bartlett, J. L., Monet, D. G., and Zacharias, M. I. (2012). VizieR Online Data Catalog: UCAC4 Catalogue (Zacharias+, 2012). *VizieR Online Data Catalog*, 1322.

Attachments

A Spectra

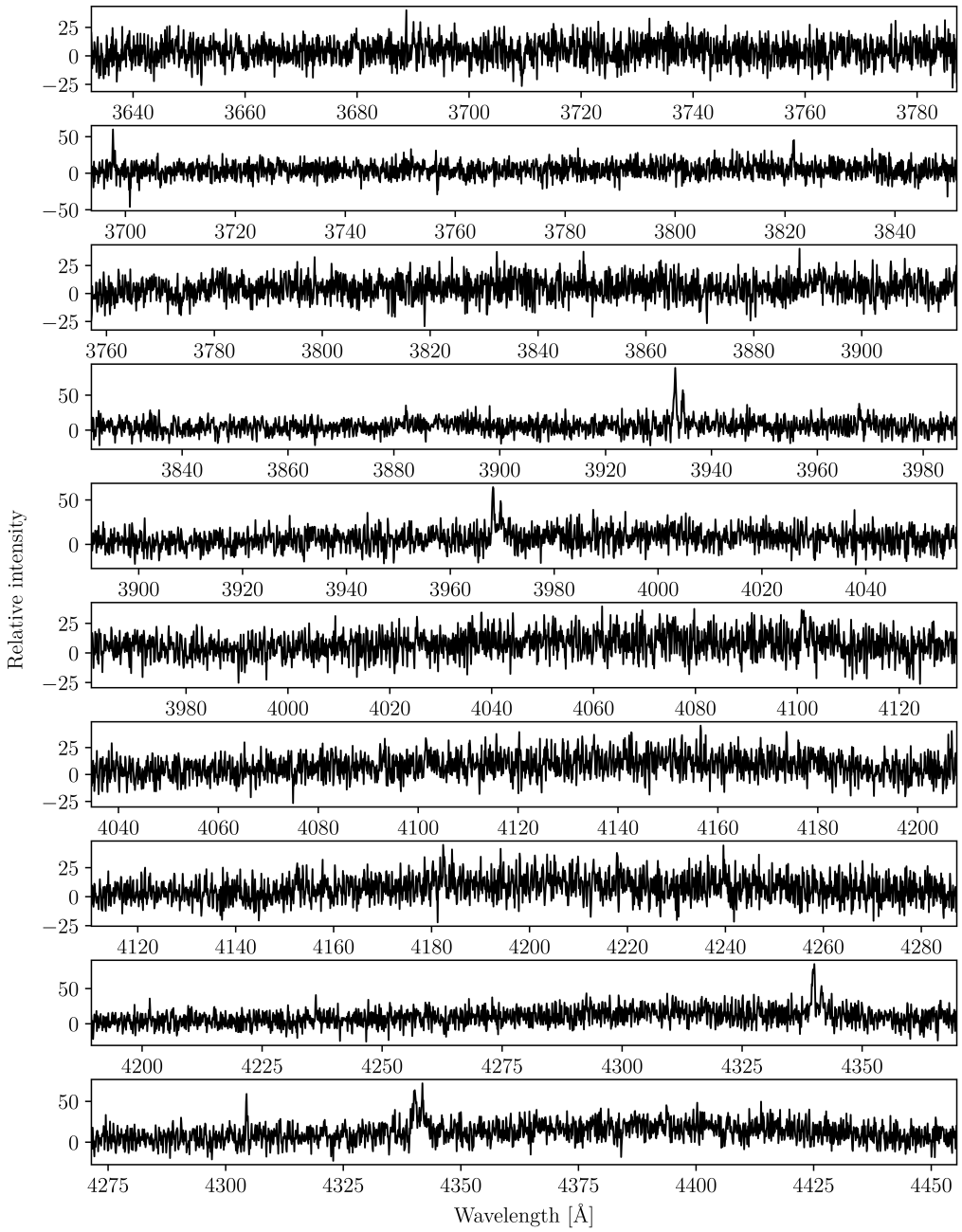

Figure A.1: Spectrum of GJ 3236 taken on the 18th November 2016. Depicted wavelengths are between 3632 Å and 4455 Å.

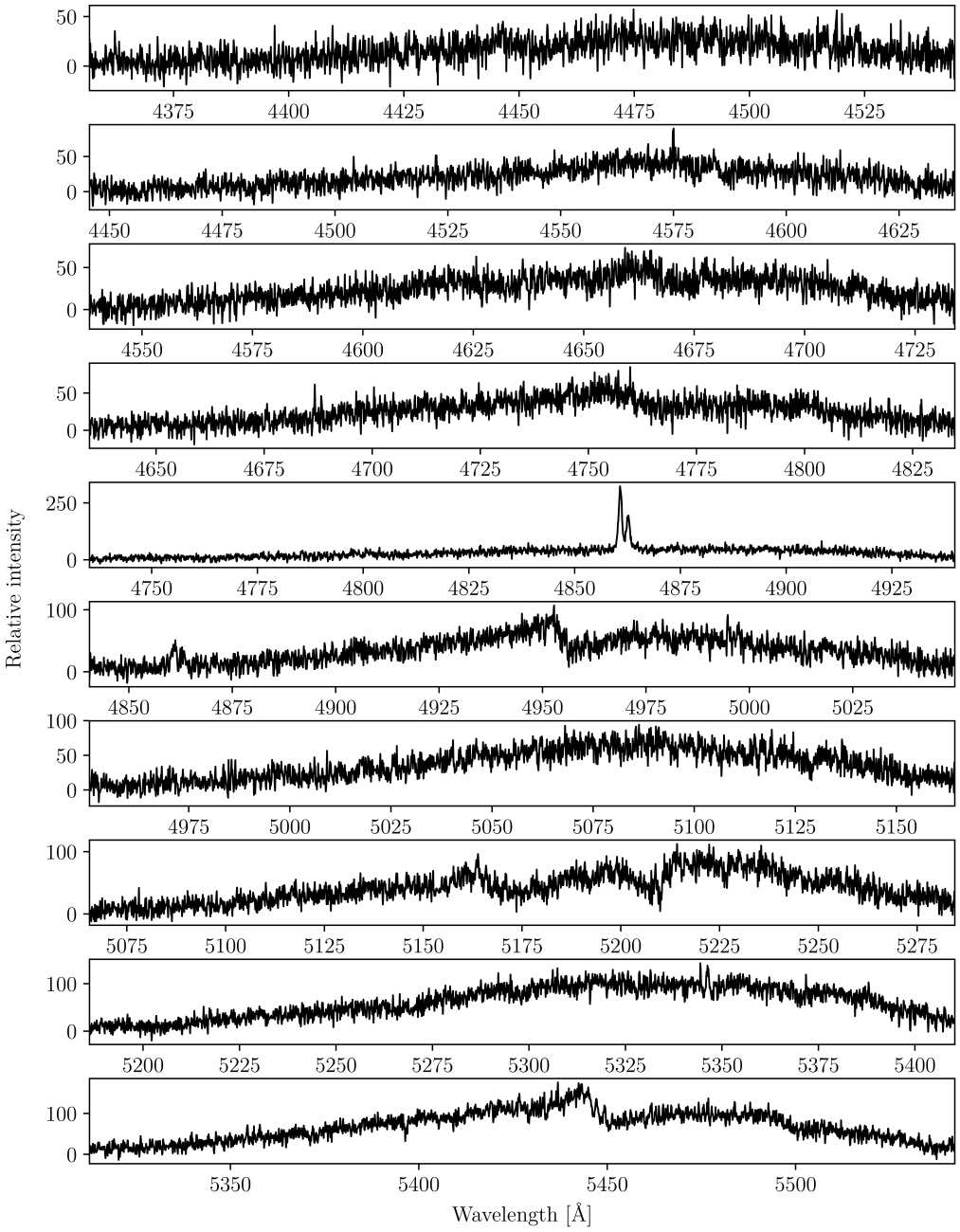

Figure A.2: Spectrum of GJ 3236 taken on the 18th November 2016. Depicted wavelengths are between 4356 Å and 5542 Å. Fifth panel from the top shows Hβ emission line.

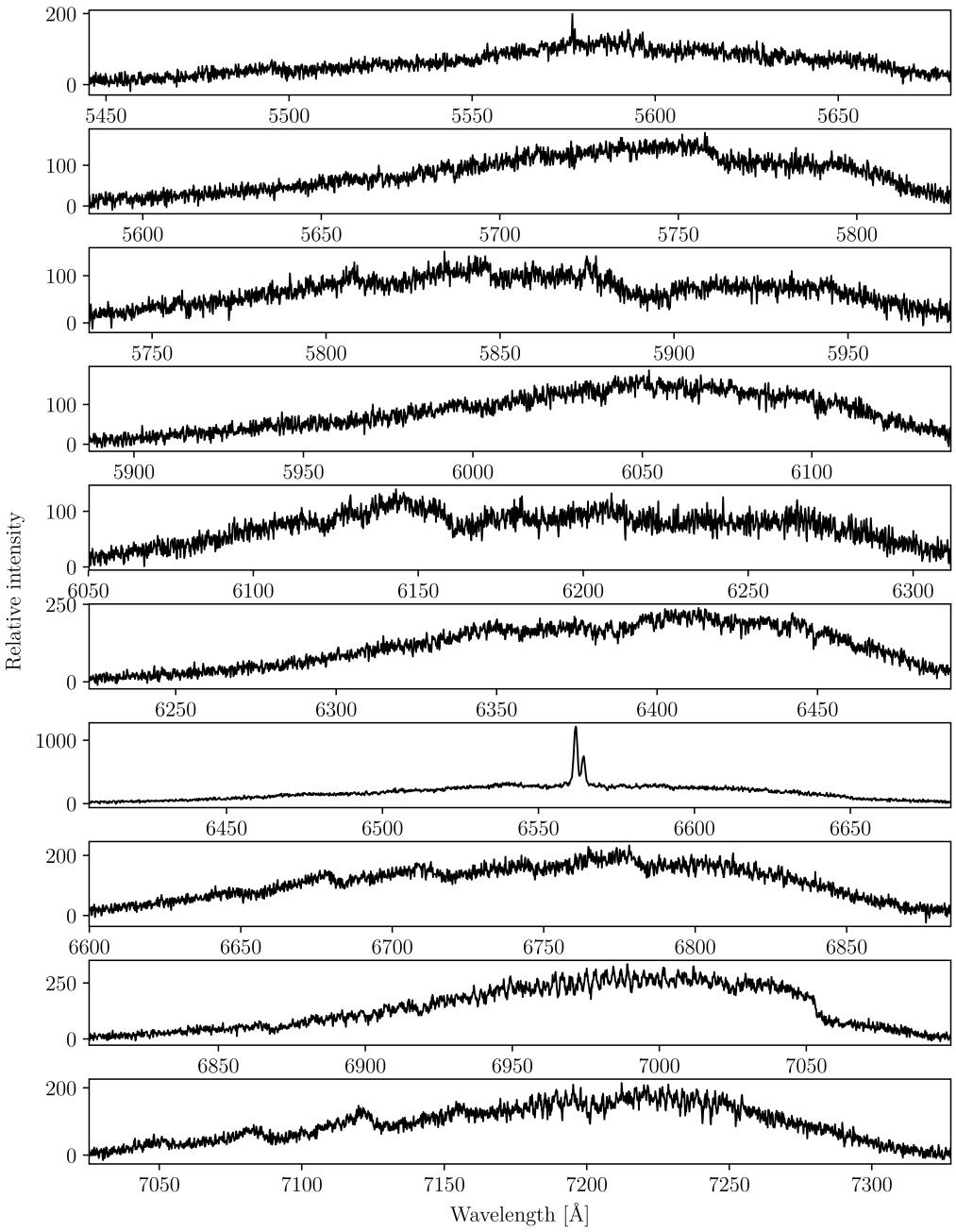

Figure A.3: Spectrum of GJ 3236 taken on the 18th November 2016. Depicted wavelengths are between 5445 Å and 7327 Å. Fourth panel from the bottom shows Hα emission line.

B Observations

Table B.1: List of observations in R filter at the Kolonické sedlo observatory.

Date	Time observed [min]	Date	Time observed [min]
23. 8. 2015	123	3. 11. 2015	426
30. 10. 2015	703	5. 11. 2015	461
31. 10. 2015	690	29. 12. 2015	514
1. 11. 2015	315	5. 2. 2016	257

Table B.2: List of observations in V filter at the Kolonické sedlo observatory.

Date	Time observed [min]	Date	Time observed [min]
24. 11. 2015	354	5. 2. 2016	255
29. 12. 2015	502		

Table B.3: List of observations in I filter at the Kolonické sedlo observatory.

Date	Time observed [min]	Date	Time observed [min]
24. 11. 2015	448		

Table B.4: List of observations in B filter at the Piszkéstetö observatory.

Date	Time observed [min]	Date	Time observed [min]
27. 11. 2016	145	21. 1. 2017	253
28. 11. 2016	342	24. 1. 2017	469
29. 11. 2016	650		

Table B.5: List of observations in R filter at the Ondřejov observatory.

Date	Time observed [min]	Date	Time observed [min]
13. 9. 2012	52	8. 1. 2014	55
30. 9. 2012	91	11. 2. 2014	65
31. 1. 2013	8	5. 4. 2014	62
6. 2. 2013	55	2. 8. 2014	142
26. 7. 2013	47	28. 8. 2014	48
27. 7. 2013	68	8. 12. 2014	180
28. 7. 2013	77	5. 8. 2015	59
16. 8. 2013	44	8. 11. 2015	565
16. 10. 2013	80	16. 11. 2015	49

Table B.6: List of observations in V filter at the Ondřejov observatory.

Date	Time observed [min]	Date	Time observed [min]
11. 11. 2015	279	28. 11. 2016	404
22. 11. 2015	393	10. 1. 2017	188
3. 12. 2015	259	26. 1. 2017	77
22. 12. 2015	215	13. 2. 2017	66
23. 12. 2015	194	15. 3. 2017	28
26. 12. 2015	334	17. 5. 2017	33
27. 12. 2015	139	31. 7. 2017	82
8. 1. 2016	207	4. 8. 2017	107
18. 1. 2016	165	7. 8. 2017	312
6. 2. 2016	253	28. 8. 2017	25
7. 3. 2016	53	15. 9. 2017	92
29. 4. 2016	151	13. 10. 2017	67
30. 4. 2016	230	14. 10. 2017	174
18. 7. 2016	36	15. 10. 2017	121
19. 7. 2016	129	16. 10. 2017	44
20. 7. 2016	112	3. 11. 2017	383
6. 8. 2016	113	4. 11. 2017	130
15. 8. 2016	27	14. 11. 2017	165
13. 9. 2016	92	16. 11. 2017	105
14. 9. 2016	405	23. 11. 2017	138
24. 9. 2016	189	1. 12. 2017	190
7. 10. 2016	181	11. 12. 2017	73
16. 10. 2016	50	26. 12. 2017	171
20. 10. 2016	139	29. 12. 2017	169
9. 11. 2016	196	6. 2. 2018	30
14. 11. 2016	183	19. 2. 2018	58
27. 11. 2016	210	20. 2. 2018	28
28. 11. 2016	438	21. 2. 2018	120

Table B.7: List of observations in R filter at the Valašské Meziříčí observatory, part 1.

Date	Time observed [min]	Date	Time observed [min]
12. 3. 2014	358	19. 10. 2014	519
13. 3. 2014	330	26. 10. 2014	286
20. 3. 2014	470	27. 10. 2014	144
21. 3. 2014	161	28. 10. 2014	507
23. 3. 2014	377	29. 10. 2014	651
25. 3. 2014	383	30. 10. 2014	107
28. 3. 2014	84	2. 11. 2014	436
29. 3. 2014	368	3. 11. 2014	176
30. 3. 2014	326	23. 11. 2014	595
1. 4. 2014	356	9. 12. 2014	439
2. 4. 2014	282	26. 12. 2014	176
3. 4. 2014	262	30. 12. 2014	313
4. 4. 2014	218	13. 1. 2015	592
7. 4. 2014	265	26. 1. 2015	241
17. 4. 2014	338	3. 2. 2015	223
23. 4. 2014	73	12. 2. 2015	561
27. 4. 2014	221	14. 2. 2015	457
30. 4. 2014	272	15. 2. 2015	375
8. 5. 2014	366	17. 2. 2015	272
12. 5. 2014	259	19. 2. 2015	65
26. 6. 2014	233	20. 2. 2015	363
6. 7. 2014	274	21. 2. 2015	492
7. 7. 2014	187	2. 3. 2015	388
13. 7. 2014	65	3. 3. 2015	322
16. 7. 2014	273	7. 3. 2015	488
18. 7. 2014	295	8. 3. 2015	433
22. 7. 2014	337	9. 3. 2015	360
14. 8. 2014	130	17. 3. 2015	483
17. 8. 2014	423	18. 3. 2015	529
21. 8. 2014	267	19. 3. 2015	453
24. 8. 2014	372	20. 3. 2015	310
28. 8. 2014	423	23. 3. 2015	388
4. 9. 2014	300	1. 7. 2015	247
8. 9. 2014	138	2. 7. 2015	244
18. 9. 2014	482	3. 7. 2015	348
23. 9. 2014	259	9. 7. 2015	202
29. 9. 2014	506	10. 7. 2015	252
6. 10. 2014	501	16. 7. 2015	284
14. 10. 2014	348	22. 7. 2015	299
18. 10. 2014	479	31. 7. 2015	118

Table B.8: List of observations in R filter at the Valašské Meziříčí observatory, part 2.

Date	Time observed [min]	Date	Time observed [min]
4. 8. 2015	290	30. 12. 2015	706
5. 8. 2015	353	8. 1. 2016	619
6. 8. 2015	419	14. 1. 2016	262
7. 8. 2015	390	21. 1. 2016	411
10. 8. 2015	144	22. 1. 2016	660
13. 8. 2015	451	24. 2. 2016	357
14. 8. 2015	237	26. 2. 2016	409
20. 8. 2015	397	16. 3. 2016	160
21. 8. 2015	389	17. 3. 2016	453
26. 8. 2015	298	19. 3. 2016	421
29. 8. 2015	405	29. 3. 2016	257
30. 8. 2015	390	2. 4. 2016	358
31. 8. 2015	220	5. 4. 2016	233
1. 9. 2015	367	6. 4. 2016	209
30. 9. 2015	420	12. 4. 2016	217
1. 10. 2015	523	21. 4. 2016	380
2. 10. 2015	605	22. 7. 2016	295
5. 10. 2015	554	8. 8. 2016	372
24. 10. 2015	546	11. 8. 2016	401
27. 10. 2015	539	18. 8. 2016	420
31. 10. 2015	555	19. 8. 2016	330
2. 11. 2015	546	22. 8. 2016	292
5. 11. 2015	534	26. 8. 2016	500
8. 11. 2015	377	27. 8. 2016	475
24. 11. 2015	712	30. 8. 2016	418
10. 12. 2015	240	31. 8. 2016	422
26. 12. 2015	582		

Table B.9: List of observations in V filter at the Valašské Meziříčí observatory.

Date	Time observed [min]	Date	Time observed [min]
5. 4. 2016	134	31. 8. 2016	400
11. 8. 2016	387	6. 10. 2016	150
30. 8. 2016	405		

Table B.10: List of observations with no filter at the Valašské Meziříčí observatory.

Date	Time observed [min]	Date	Time observed [min]
21. 1. 2017	781	15. 10. 2017	333
25. 8. 2017	393 1	6. 10. 2017	463

Table B.11: List of observations with no filter at the Trhové Sviny observatory.

Date	Time observed [min]	Date	Time observed [min]
27. 12. 2015	770	29. 11. 2016	710
28. 12. 2015	417	2. 12. 2016	795
30. 12. 2015	621	3. 12. 2016	632
29. 1. 2016	357	10. 12. 2016	729
6. 2. 2016	450	16. 12. 2016	581
11. 2. 2016	545	30. 12. 2016	771
24. 2. 2016	430	31. 12. 2016	740
26. 2. 2016	434	1. 1. 2017	715
27. 2. 2016	499	10. 1. 2017	629
17. 3. 2016	567	18. 1. 2017	446
18. 3. 2016	517	19. 1. 2017	642
1. 4. 2016	490	20. 1. 2017	637
26. 8. 2016	490	21. 1. 2017	646
27. 8. 2016	499	22. 1. 2017	656
28. 8. 2016	218	13. 2. 2017	612
30. 8. 2016	492	15. 2. 2017	609
31. 8. 2016	513	27. 2. 2017	378
1. 9. 2016	354	25. 8. 2017	342
2. 9. 2016	504	28. 8. 2017	493
7. 9. 2016	527	29. 8. 2017	498
8. 9. 2016	536	8. 9. 2017	536
10. 9. 2016	536	29. 9. 2017	613
12. 9. 2016	534	30. 9. 2017	625
13. 9. 2016	535	15. 10. 2017	624
14. 9. 2016	462	16. 10. 2017	632
15. 9. 2016	495	19. 10. 2017	582
24. 9. 2016	484	30. 10. 2017	160
25. 9. 2016	525	3. 11. 2017	730
26. 9. 2016	516	15. 11. 2017	367
27. 9. 2016	458	22. 11. 2017	681
29. 9. 2016	532	23. 11. 2017	704
4. 10. 2016	379	6. 12. 2017	744
31. 10. 2016	256	7. 12. 2017	564
13. 11. 2016	567	24. 12. 2017	814
17. 11. 2016	280	25. 12. 2017	786
21. 11. 2016	293		

C List of observed flares

Table C.12: List of observed flares. Heliocentric Julian date corresponds to the maximal brightness of the flare. Names of observatories are shortened to O (Ondřejov), VM (Valašské Meziříčí), TS (Trhové Sviny), KS (Kolonické sedlo) and P (Piszkéstetö), photometric filter used for observations are also given in the table.

Number	Date	HJD −2400000	Observatory
1	6. 2. 2013	56330.33225	O-R
2	27. 7. 2013	56501.55930	O-R
3	8. 1. 2014	56666.21790	O-R
4	2. 8. 2014	56872.46826	O-R
5		56872.47242	O-R
6	20. 3. 2014	56737.41890	VM-R
7		56737.43401	VM-R
8	17. 4. 2014	56765.47048	VM-R
9	22. 7. 2014	56861.35532	VM-R
10	14. 8. 2014	56884.38779	VM-R
11	17. 8. 2014	56887.52320	VM-R
12	6. 10. 2014	56937.48295	VM-R
13	19. 10. 2014	56950.45316	VM-R
14	29. 10. 2014	56960.21508	VM-R
15		56960.25395	VM-R
16		56960.31837	VM-R
17		56960.52327	VM-R
18	23. 11. 2014	56985.26845	VM-R
19		56985.32286	VM-R
20	13. 1. 2015	57036.52115	VM-R
21	12. 2. 2015	57066.48844	VM-R
22	15. 2. 2015	57069.46653	VM-R
23	3. 3. 2015	57085.33289	VM-R
24	19. 3. 2015	57101.29758	VM-R
25	20. 3. 2015	57102.34356	VM-R
26	23. 3. 2015	57105.42391	VM-R
27		57105.43521	VM-R
28	4. 8. 2015	57239.40341	VM-R
29	30. 8. 2015	57265.52174	VM-R
30	30. 9. 2015	57296.34121	VM-R
31		57296.42895	VM-R
32		57296.50182	VM-R
33	2. 10. 2015	57298.51308	VM-R
34		57298.53791	VM-R
35	5. 10. 2015	57301.36681	VM-R
36		57301.48144	VM-R
37	24. 10. 2015	57320.39855	VM-R
38	31. 10. 2015	57327.48196	KS-R

Table C.12: (continued)

No.	Date	HJD −2400000	Observatory
39	3. 11. 2015	57330.28911	KS-R
40	5. 11. 2015	57332.38291	VM-R, KS-R
41		57332.44575	KS-R
42	8. 11. 2015	57335.43925	O-R
43		57335.45855	O-R
44	11. 11. 2015	57338.30788	O-V
45		57338.41351	O-V
46		57338.45907	O-V
47	22. 11. 2015	57349.31266	O-V
48		57349.42577	O-V
49		57349.51647	O-V
50	24. 11. 2015	57351.43346	VM-R, KS-V
51		57351.62977	VM-R
52	3. 12. 2015	57360.41228	O-V
53		57360.43124	O-V
54	22. 12. 2015	57379.35554	O-V
55		57379.37719	O-V
56		57379.38553	O-V
57	23. 12. 2015	57380.41235	O-V
58		57380.43749	O-V
59	27. 12. 2015	57384.23648	O-V, TS-C
60		57384.25998	TS-C
61		57384.46139	TS-C
62		57384.64811	TS-C
63		57384.67053	TS-C
64	8. 1. 2016	57396.34824	O-V, VM-R
65		57396.46788	VM-R
66	22. 1. 2016	57410.48126	VM-R
67	5. 2. 2016	57424.30481	KS-V
68		57424.32897	KS-R, KS-V
69	24. 2. 2016	57443.25743	TS-C
70		57443.44307	VM-R, TS-C
71		57443.47294	TS-C
72	26. 2. 2016	57445.55347	VM-R
73	27. 2. 2016	57446.23113	TS-C
74		57446.26420	TS-C
75		57446.33353	TS-C
76		57446.45943	TS-C
77	17. 3. 2016	57465.31947	VM-R, TS-C
78	5. 4. 2016	57484.37494	VM-R, VM-V
79	21. 4. 2016	57500.32473	VM-R
80		57500.33675	VM-R
81		57500.48869	VM-R
82	19. 7. 2016	57589.39177	O-V
83	6. 8. 2016	57607.53174	O-V

Table C.12: (continued)

No.	Date	HJD −2400000	Observatory
84	11. 8. 2016	57612.32248	VM-R, VM-V
85		57612.36863	VM-V
86	26. 8. 2016	57627.61020	TS-C
87	27. 8. 2016	57628.35173	VM-R
88		57628.36091	VM-R
89		57628.36939	VM-R
90		57628.38539	TS-C
91	28. 8. 2016	57629.32385	TS-C
92		57629.34093	TS-C
93	30. 8. 2016	57631.44610	VM-R, TS-C
94		57631.51322	VM-R, VM-V, TS-C
95	31. 8. 2016	57632.43564	VM-R, VM-V, TS-C
96	1. 9. 2016	57633.52323	TS-C
97	7. 9. 2016	57639.44980	TS-C
98		57639.51808	TS-C
99	8. 9. 2016	57640.58189	TS-C
100	10. 9. 2016	57642.43108	TS-C
101		57642.46735	TS-C
102	12. 9. 2016	57644.30381	TS-C
103		57644.45265	TS-C
104		57644.46766	TS-C
105	13. 9. 2016	57645.32637	O-V, TS-C
106		57645.43088	TS-C
107		57645.59306	TS-C
108	14. 9. 2016	57646.43144	O-V, TS-C
109		57646.48880	O-V, TS-C
110		57646.51349	O-V
111	24. 9. 2016	57656.27344	TS-C
112	25. 9. 2016	57657.55836	TS-C
113	27. 9. 2016	57659.54082	TS-C
114	29. 9. 2016	57661.37455	TS-C
115	6. 10. 2016	57668.25916	VM-V, TS-C
116	7. 10. 2016	57669.29398	O-V
117	31. 10. 2016	57693.21571	TS-C
118		57693.24132	TS-C
119	13. 11. 2016	57706.27890	TS-C
120		57706.29384	TS-C
121	21. 11. 2016	57714.34314	TS-C
122	27. 11. 2016	57720.49260	O-V
123		57720.50018	O-V
124		57720.61019	P-B
125		57720.64930	P-B
126		57720.69155	P-B
127	28. 11. 2016	57721.20205	P-B
128		57721.21318	P-B

Table C.12: (continued)

No.	Date	HJD −2400000	Observatory
129		57721.22430	P-B
130		57721.23098	P-B
131		57721.23616	P-B
132		57721.25544	P-B
133		57721.29177	P-B
134		57721.64966	O-V, P-B
135		57721.68896	P-B
136		57721.69044	P-B
137	29. 11. 2016	57722.24224	P-B
138		57722.26010	P-B
139		57722.38817	P-B
140		57722.43074	P-B
141		57722.43839	P-B
142		57722.44146	P-B
143		57722.45013	P-B
144		57722.45574	P-B
145		57722.45829	P-B
146		57722.48636	P-B
147		57722.54112	P-B
148		57722.54776	P-B
149		57722.56640	TS-C, P-B
150		57722.60347	P-B
151		57722.65040	P-B
152		57722.67540	P-B
153		57722.68102	P-B
154	2. 12. 2016	57725.53647	TS-C
155	3. 12. 2016	57726.43351	TS-C
156	10. 12. 2016	57733.56214	TS-C
157		57733.63149	TS-C
158		57733.63789	TS-C
159	16. 12. 2016	57739.19640	TS-C
160	30. 12. 2016	57753.27216	TS-C
161		57753.40234	TS-C
162		57753.61575	TS-C
163		57753.67229	TS-C
164	31. 12. 2016	57754.44775	TS-C
165	10. 1. 2017	57764.39115	O-V
166	20. 1. 2017	57774.51029	TS-C
167		57774.54454	TS-C
168	21. 1. 2017	57775.21485	P-B
169		57775.28420	P-B
170		57775.28588	P-B
171		57775.39995	P-B
172		57775.44080	VM-C, TS-C, P-B
173	22. 1. 2017	57776.52020	TS-C

Table C.12: (continued)

No.	Date	HJD −2400000	Observatory
174	24. 1. 2017	57778.19457	P-B
175		57778.21193	P-B
176		57778.27523	P-B
177		57778.36963	P-B
178		57778.56009	P-B
179		57778.59729	P-B
180	26. 1. 2017	57780.29709	O-V
181	15. 2. 2017	57800.47940	TS-C
182	27. 2. 2017	57812.25799	TS-C
183	4. 8. 2017	57970.38999	O-V
184	7. 8. 2017	57973.49968	O-V
185	25. 8. 2017	57991.42297	VM-C, TS-C
186	28. 8. 2017	57994.28669	TS-C
187		57994.29096	TS-C
188		57994.30056	TS-C
189		57994.31443	TS-C
190		57994.31764	TS-C
191		57994.43503	TS-C
192		57994.55133	O-V
193		57994.58228	TS-C
194		57994.58655	TS-C
195	29. 8. 2017	57995.29628	TS-C
196	8. 9. 2017	58005.32863	TS-C
197	29. 9. 2017	58026.32047	TS-C
198		58026.35142	TS-C
199		58026.48801	TS-C
200		58026.51895	TS-C
201	15. 10. 2017	58042.43254	VM-C, TS-C
202		58042.49127	O-V, TS-C
203		58042.49809	O-V, TS-C
204		58042.50643	O-V, TS-C
205		58042.52387	O-V
206		58042.52936	O-V, TS-C
207		58042.53922	O-V
208	16. 10. 2017	58043.21795	VM-C, TS-C
209		58043.37324	VM-C, TS-C
210		58043.50769	TS-C
211		58043.55677	TS-C
212		58043.61440	TS-C
213	3. 11. 2017	58061.39713	TS-C
214		58061.41278	O-V, TS-C
215		58061.44766	O-V, TS-C
216		58061.49620	O-V, TS-C
217	4. 11. 2017	58062.44060	O-V
218		58062.46637	O-V

Table C.12: (continued)

No.	Date	HJD −2400000	Observatory
219	14. 11. 2017	58072.33972	O-V
220	16. 11. 2017	58074.38233	O-V
221	22. 11. 2017	58080.20626	TS-C
222		58080.26390	TS-C
223		58080.36102	TS-C
224		58080.43038	TS-C
225		58080.53817	TS-C
226	6. 12. 2017	58094.60980	TS-C
227	7. 12. 2017	58095.52495	TS-C
228	24. 12. 2017	58112.35920	TS-C
229		58112.41152	TS-C
230		58112.43605	TS-C
231		58112.47553	TS-C
232		58112.57799	TS-C
233		58112.68576	TS-C
234		58112.69431	TS-C
235		58112.69644	TS-C
236		58112.70071	TS-C
237		58112.70604	TS-C
238		58112.71992	TS-C
239	25. 12. 2017	58113.24329	TS-C
240		58113.57322	TS-C
241		58113.68213	TS-C

D Energy estimation script

An example of a script written in the PYTHON3 programming language used for energy estimation of flares observed at the Piszkéstetö Observatory using B photometric filter.

```
# Libraries
import matplotlib.pyplot as plt
import numpy as np
from scipy import integrate
from scipy.interpolate import interp1d

# Import of the data from a file
file = input('File containing flare: ')
dat1 = np.loadtxt(file)
x1 = dat1[:, 0]
y1 = dat1[:, 1]

n = np.argmin(y1)
time = x1[n]
print('Time:', time)
x1 = x1 - min(x1)

# Printing of the amplitudes with respect to the
# lowest point of measurements and last and first point
ampl = max(y1)-min(y1)
print('Amplitude (max-min) [mag]:', round(ampl,2))
ampl = y1[-1] - min(y1)
print('Amplitude (max-last) [mag]:', round(ampl,2))
ampl = y1[0] - min(y1)
print('Amplitude (max-first) [mag]:', round(ampl,2))

# Conversion from magnitudes to luminosities
mag_0 = 0.25
L_0 = 9.09 * 0.0127149219149
y_int = L_0 * ((10**(-0.4*(y1-mag_0)))-1)

# Fitting spline function
f_spline = interp1d(x1, y_int, kind='cubic')

min_x = min(x1)
max_x = max(x1)

x_new = np.linspace(min_x, max_x, num=10000, endpoint=True)
y_opt = f_spline(x_new)
t_s = x_new*24*3600

# Integration of the spline function
int_flare = integrate.simps(y_opt, t_s)

# Printing of the flare duration in minutes
t_flare = max(t_s)-min(t_s)
```

```
print('Duration [min]:',int(round(t_flare/60,0)))

# Printing of the energy estimation
int_flare = int_flare - t_flare * y_int[0]
print('Energy [e25 J]:', round(int_flare/10,2))

# Plotting of the light curve for revision
plt.scatter(x1, y_int, color='blue', s=10, zorder=2)
plt.plot(x_new, f_spline(x_new), zorder=1)
plt.scatter(x1[n], y_int[n], color='red', s=10, zorder=3)
plt.show()
```